

Adversarial Attack and Defense for Dehazing Networks

Jie Gui, Xiaofeng Cong, Chengwei Peng, Yuan Yan Tang, James Tin-Yau Kwok

Abstract—The research on single image dehazing task has been widely explored. However, as far as we know, no comprehensive study has been conducted on the robustness of the well-trained dehazing models. Therefore, there is no evidence that the dehazing networks can resist malicious attacks. In this paper, we focus on designing a group of attack methods based on first order gradient to verify the robustness of the existing dehazing algorithms. By analyzing the general goal of image dehazing task, five attack methods are proposed, which are prediction, noise, mask, ground-truth and input attack. The corresponding experiments are conducted on six datasets with different scales. Further, the defense strategy based on adversarial training is adopted for reducing the negative effects caused by malicious attacks. In summary, this paper defines a new challenging problem for image dehazing area, which can be called as adversarial attack on dehazing networks (AADN). Code is available at <https://github.com/guijie/AADN>.

Index Terms—Image dehazing, adversarial attack and defense, security, first order gradient.

I. INTRODUCTION

THE goal of image dehazing is to restore the clear scene from the hazy image [1]–[3], which is an important topic on low-level computer vision tasks [4]. However, the security of dehazing algorithms has not received due attention. In this paper, we find that well-trained dehazing networks with high performance can be fooled by the attack methods based on first order gradient [5].

Various dehazing networks have been proposed, such as AODNet [6], DM2FNet [7], MSBDN [8], FFANet [9], Grid-DehazeNet [10] and 4KDehazing [11]. These networks use different loss functions, network blocks and training strategies during the training stage, but share the same process during the inference stage. In this paper, we focus on the single input single output (SISO) dehazing systems, which take one

hazy image as input and provide one dehazed image as output without estimating transmission map and atmospheric light in an explicit way during the inference stage. Within the scope of this study, we argue that SISO dehazing networks can be attacked by unified malicious attack algorithms [12], [13].

In addition, we propose two questions for adversarial attack on dehazing networks (AADN) research as follows.

- Can the state-of-the-art dehazing models be attacked? How can we attack them?
- If the dehazing models are vulnerable, how can we protect them in a proper way?

From the attacker’s perspective, unlike the class-based image classification task, the outputs of dehazing network are in pixel-wise form. The main difficulty is that the attacker may not have the “ground truth labels” for attacking. Therefore, we propose several attack methods that can avoid using the ground truth labels. After finding that the dehazing networks can be attacked by the first order attack algorithm, a natural question is whether we can design a corresponding defense method to improve the performance after being attacked. Inspired by the research on robust image classification [5], an adversarial training strategy is adopted for defense process. The main contributions of this paper are as follows.

- We define a new valuable research area called AADN. A pixel-wise white-box [14], [15] attack form is proposed for image dehazing task as the basic attack form, which is based on the gradient information during the back propagation process.
- By analyzing the characteristics of SISO dehazing task, five attack methods are designed and verified on six benchmark datasets.
- To explore if the attack effects can be reduced, the adversarial training are used for protecting the dehazing models with the target guiding way. Further, we find that adversarial defense training can improve the robustness of dehazing networks, but it can not “perfectly” protect the dehazing networks. After defense training, the dehazing networks can be still attacked by attacker. Such conclusion is consistent with the research on the attack and defense on image classification [5].

Our research shows that the SISO dehazing models can be attacked by first-order gradient-based attack algorithm. Furthermore, we get three important conclusions. First, adversarial perturbations acquired with gradient information have significantly stronger negative effects on the dehazing model than regular noises. Second, the attacker only needs to use the outputs of dehazing models as pseudo-labels instead of using

We thank the Big Data Computing Center of Southeast University for providing the facility support on the numerical calculations in this paper. This work was supported in part by National Key R&D Program of China under Grant 2022YFB3104301; the grant of the National Science Foundation of China under Grant 62172090; the Fundamental Research Funds for the Central Universities; CAAI-Huawei MindSpore Open Fund. All correspondence should be directed to Xiaofeng Cong.

J. Gui is with the School of Cyber Science and Engineering, Southeast University and with Purple Mountain Laboratories, Nanjing 210000, China (e-mail: guijie@seu.edu.cn).

X. Cong is with the School of Cyber Science and Engineering, Southeast University, Nanjing 210000, China (e-mail: cxf_svip@163.com).

C. Peng is with the Tencent Company, Shenzhen 518000, China (e-mail: cwpeng@tencent.com).

Y. Tang is with the Department of Computer and Information Science, University of Macao, Macao 999078, China (e-mail: yuanyant@gmail.com).

J. Kwok is with the Department of Computer Science and Engineering, The Hong Kong University of Science and Technology, Hong Kong 999077, China. (e-mail: jamesk@cse.ust.hk).

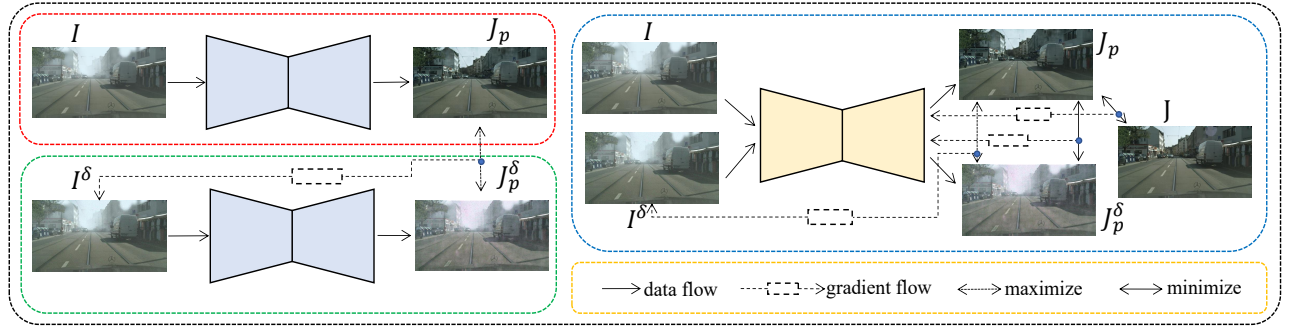


Fig. 1. The pipelines of adversarial attack and defense on AADN. The contents of the four dotted boxes are (a) original dehazing process (upper left), (b) attack dehazing network (lower left), (c) adversarial defense training (upper right), and (d) illustration of arrows (lower right), respectively.

the ground-truth haze-free images as the guidance information for the attack process. Third, adversarial defense training can reduce the negative impacts caused by the attack algorithm, but it cannot completely eliminate these impacts. Meanwhile, adversarial defense training will slightly reduce the dehazing performance of the dehazing model on normal examples.

II. RELATED WORK

A. Image Dehazing

Image dehazing algorithms aim at removing the haze on the hazy images [1], [2], [16]–[19]. The existing dehazing methods can be divided into DL-based and non-DL-based [4]. Overall, without considering the computation cost, the DL-based dehazing methods can achieve better performance than non-DL-based methods. However, our research shows the DL-based SISO dehazing models can be attacked by the first order attack algorithms.

Various dehazing networks have been proposed by the researchers. A reformulated atmospheric scattering model is embedded to AODNet [6], which is a light weight dehazing network. GCANet [20] utilizes the idea of residual learning, which can promote the dehazing performance. DM2FNet [7] adopts five different feature functions and fuses them to the final output. The attention mechanism is applied in FFANet [9] and GridDehazeNet [10], which can obtain fine dehazing results. MSBDN [8] prove that boosting strategy and back projection can be used in dehazing module, which can preserve spatial information by a symmetrical path. The contrastive learning is used for dehazing task by AECR-Net [21], which constructs the positive and negative pairs during training process. DIDH [22] proposes to restore the high frequency and low frequency information by discriminator networks. RDN [23] proves that retinex model can be embedded to the dehazing process to obtain the residual illumination map and the dehazed image. PSD [24] takes a pre-trained and fine-tuning strategy to utilize the physical priors. DeHamer [25] uses the transformer architecture to implement the dehazing network. 4KDehazing [11] puts affine bilateral grid learning as a branch to the overall network that can process the high resolution image with high speed. Within the scope of SISO dehazing system, we find these well-known dehazing networks can be fooled by first order attack.

B. Adversarial Attack and Defense

The adversarial attack and defense are important topics for artificial intelligence security [26]–[30]. It is an interesting question to evaluate the robustness of neural networks under attack [31]. The research on adversarial attack argue that the well-trained networks may be fooled by hostile attack [12], [32]. By adding small perturbation to the example, the prediction label generated by the classification network may change from “panda” (correct) to “gibbon” (incorrect) [12].

Goodfellow proposes a fast gradient sign method (FGSM) [33] to generate the perturbation. FGSM is a one-step attack method which utilizes the gradient information calculated by the back propagation process. An iteration-based fast gradient sign method (i-FGSM) inspired by FGSM is explored by Kurakin et al. [34]. Instead of generating the perturbation by one step backward like FGSM, i-FGSM update the perturbation by multi-step and clip it into a fixed range. Besides, projected gradient descent (PGD) [5] is also a promising attack method to obtain adversarial example that uses multi-step update strategy. Inspired by PGD and [35], the methods for attacking the dehazing networks are proposed in this paper.

Recent research has explored the topic on adversarial attack on image deraining [35], semantic segmentation [36], [37], super-resolution [38]–[40] and deblurring [41]. Gao et al. [42] invent an adversarial haze synthetic process based on atmospheric scattering model to fool the classifiers. Kanwal et al. [43] study how to use the haze to reduce or improve the performance of person re-identification task. Sun et al. [44] propose a targeted adversarial attack to boost object detection performance after restoration. The goal of [42]–[44] are different from this paper, since our purpose is to attack the dehazing networks. To the best of our knowledge, no comprehensive research on the dehazing adversarial attack has been published yet.

This paper focuses on white-box attack. White-box attack, gray-box attack and black-box attack are popular research areas currently [14], [15]. White-box attack assumes the information of the networks can be obtained, like architecture and parameters. Gray-box attack and black-box attack assume the information is partially knowable and completely unknowable, respectively. In addition, [5], [45] propose to treat the adversarial attack and defense as a game theoretic framework.

In our experiments, we try to protect the dehazing network by adversarial training from the white-box attack.

III. METHODS

The important concepts for AADN are as follows, which are consistent with the whole paper.

- Attack: a process trying to reduce the performance of the well-trained dehazing networks by adding subtle perturbation to the hazy image.
- Attacker: a hostile attack algorithm, which can generate adversarial perturbation.
- Perturbation: a subtle signal generated by the attacker, and it is added to the hazy image.
- Adversarial example: a hazy image with perturbations.
- Defense: a process that tries to reduce the negative effects caused by the attacker.

The hazy image is denoted as I and the corresponding ground truth haze-free image is marked as J . J_p stands for the predicted dehazed image obtained by dehazing network.

There are three important parts in this section. Basic attack form is introduced in Subsection III-A, which defines the general way to attack the SISO dehazing system. Subsection III-B describes five attack methods to disturb the dehazing networks. Subsection III-C shows the adversarial training defense strategy to obtain robust dehazing networks.

A. Basic Attack Form

The process of attacking the dehazing network is to add a perturbation δ to a hazy image I and to obtain the adversarial example I^δ , and this behavior makes the output (J_p^δ) of dehazing network unpleasant, as follows,

$$J_p = \Gamma_\theta(I), \quad (1)$$

$$J_p^\delta = \Gamma_\theta(I + \delta) = \Gamma_\theta(I^\delta), \quad (2)$$

where Γ_θ denotes the pre-trained dehazing network with parameters θ . The general optimization goal of image dehazing algorithms is to minimize one or more distance metrics, such as L1, L2, Perceptual [46] and SSIM [47]. Therefore, the attacker tries to maximize these distance metrics, which will make the well-converged network have a higher loss value. The loss function L_{att} that the attacker adopted is to maximize

$$L_{att} = \Re(J_p^\delta, X), \quad (3)$$

where the \Re represents various loss functions for image restoration process and X is the target that the attacker needs to use. During the attack process, the parameters θ of the network Γ_θ will not be updated. The attacker needs to learn the perturbation δ , which is updated by the gradient values

$$\delta^{t+1} = \delta^t + \alpha \text{sgn}(\nabla_\delta L_{att}), \quad (4)$$

where sgn is the sign function, α is the adjusting factor for updating process, ∇ denotes gradient operation, and the t denotes t -th iteration step. For each iteration, the input I^δ of Γ_θ is not static, which is changed by the perturbation. To ensure that the perturbation δ added to hazy image I can not be easily observed, the value range of δ should be controlled.

As proposed in [5], δ can be constrained by ℓ_∞ . Further, δ will be clipped as

$$\delta^{t+1} = \kappa_{(-\epsilon, \epsilon)}(\delta^{t+1}), \quad (5)$$

where the κ stands for clip operation and ϵ represents the range for clipping. $\epsilon = 0$ denotes no attack. The pixel values of all images are normalized to $[0, 1]$ during the train and inference stage. Therefore, the value range of attacked hazy image I^δ should also be limited to $[0, 1]$, so δ is further clipped by

$$\delta^{t+1} = \kappa_{(0-I, 1-I)}(\delta^{t+1}). \quad (6)$$

The above attack form can be used in both targeted and non-targeted ways. The aim of targeted attack is forcing J_p^δ close to X . The goal of non-targeted attack is trying to make J_p^δ far from J visually.

B. How to Attack

Subsection III-A gives the basic form about how to attack the dehazing networks. Here, considering the general goal of dehazing task, five attack methods are designed, which are denoted as L_P , L_M , L_G , A_N and L_I , respectively.

1) *Attack by the Predicted Dehazed Image*: Unlike image classification or semantic segmentation tasks, the ground truth labels are not easy to be collected in dehazing task. The hazy and haze-free pairs may not be annotated by humans. Therefore, we design an attack method based on predicted dehazed image J_p that is obtained by the dehazing network Γ_θ . The loss of the attack can be expressed by

$$L_P = \Re(\Gamma_\theta(I^\delta), J_p), \quad (7)$$

where P in L_P denotes prediction. The optimization goal is to maximize L_P in a non-targeted way. Since such an attack method is non-targeted, a natural question is whether L_P will cause the prediction result $\Gamma_\theta(I^\delta)$ after the attack to be closer to the ground truth image and whether it will lead to a failure attack. The experiments show that L_P is a reliable and powerful attack method. The details can be found in the experiment part.

The original dehazing process is shown in Figure 1 (a), and the process of attacking dehazing networks is displayed in Figure 1 (b).

2) *Haze Mask Attack*: Equation (7) provides an attack way based on the whole image. An interesting question is whether we can attack part of the hazy image and achieve impressive attack results. According to the atmospheric scattering model [48], [49], the haze density of the pixels that are far from the camera is higher. This means that the haze is not always uniformly distributed across the image. Therefore, we propose the haze mask attack method which can partly attack the haze image, and the corresponding haze mask can be obtained by

$$\mu = \frac{1}{H \times W} \sum_{m=1}^H \sum_{n=1}^W (I(m, n) - J_p(m, n)), \quad (8)$$

$$\text{mask} = \begin{cases} 1 & (I(m, n) - J_p(m, n)) > \mu, \\ 0 & (I(m, n) - J_p(m, n)) \leq \mu, \end{cases} \quad (9)$$

where H and W denotes the height and width of the image, respectively. The loss function of haze mask attack is to maximize

$$L_M = \mathbb{R}(\Gamma_\theta(I + \delta * mask), J_p), \quad (10)$$

where $*$ denotes pixel-wise multiplication and M in L_M stands for the mask.

3) *Attack by the Ground Truth Clear Image:* Supposing the attacker already has the ground truth clear image J , then the J_p in attack loss L_P can be replaced with J . The attack loss calculated by J is $L_G = \mathbb{R}(\Gamma_\theta(I^\delta), J)$, where G means ground truth.

4) *Noise Attack:* The perturbation generated by the attacker can be seen as a specific noise information that is added to the hazy image. Therefore, we need to compare the attack results between the perturbation and the general noise to verify the effectiveness of the adversarial attack. The noise attack is marked as A_N , where N denotes the noise sampling from noise distribution. It is worth noting that A_N directly generates the δ by noise distribution, rather than using gradient descent algorithm. The A_N is mainly used to prove that the learned perturbation has stronger attack effects than general noise. Details can be found in experiment section.

5) *Identity Attack:* Considering an extreme situation that the output of dehazing model totally contains the haze in original hazy image. In this situation, the optimization object of the attacker is to minimize the distance between the dehazed image and the original hazy image. The loss function for identity attack is to maximize the following loss function

$$L_I = -1 * \mathbb{R}(\Gamma_\theta(I^\delta), I), \quad (11)$$

where the subscript in L_I means identity.

6) *The Distance Metrics:* The above attack objectives are all pixel-wise. Here we choose two distance metrics for $\mathbb{R}(\cdot, \cdot)$, which are mean square error (MSE) and structural similarity [47] (SSIM). The forms of MSE and SSIM are

$$MSE(x, y) = \|x - y\|_2^2, \quad (12)$$

$$SSIM(x, y) = \frac{(2\mu_x\mu_y + C1)(2\delta_{xy} + C2)}{(\mu_x^2 + \mu_y^2 + C1)(\delta_x^2 + \delta_y^2 + C2)}, \quad (13)$$

where x and y represent two images. $C1$ and $C2$ are constants. Details about SSIM can be found at [47]. The μ_x & μ_y and δ_x & δ_y denote mean and standard deviation, respectively. δ_{xy} is covariance. For convenience, the L_P^{MSE} and L_P^{SSIM} stand for the L_P that using $MSE(x, y)$ and $1 - SSIM(x, y)$ as the loss function, respectively.

C. How to Defense

The attacker that adopts white-box attack method can reduce the performance of the well-trained dehazing models. Therefore, we need to design the corresponding defense method to protect the vulnerable networks. There are two factors that we mainly consider.

- The defense method can be adopted by different dehazing models, rather than designed for a specific one.
- The inference time should not be increased by the defense method.

Algorithm 1 The maximum number of iterations is set to N . The learning rate is denoted as lr . The iteration step of attack process is k . m is batch size.

Initialize the dehazing network Γ_θ and Teacher network Γ_θ^T by well-trained parameters.

for the maximum number of iterations N **do**

Sample hazy images $I = \{i^{(1)}, i^{(2)}, \dots, i^{(m)}\}$ and corresponding ground truth images $J = \{j^{(1)}, j^{(2)}, \dots, j^{(m)}\}$;

Calculate the corresponding prediction $J_p^T = \{j_p^{T(1)}, j_p^{T(2)}, \dots, j_p^{T(m)}\}$ by $J_p^T = \Gamma_\theta^T(I)$. (14)

Initialize δ by uniform distribution $U(-\epsilon, \epsilon)$ and δ is clipped by Equation (6);

for k steps **do**

Calculate the attack loss L_P ;

Update δ by Equations (4), (5) and (6).

end for

Generate the attacked prediction J_p^δ by Equation (2);

Calculate the adversarial training loss L_{def}^P ;

Update parameters θ for Γ_θ :

$$\theta = \theta - lr \times \nabla_\theta L_{def}^P. \quad (15)$$

end for

Algorithm 2 The maximum number of iterations is set to N . The learning rate is denoted as lr . The iteration step of attack process is k . m is batch size.

Initialize the dehazing network Γ_θ by well-trained parameters.

for the maximum number of iterations N **do**

Sample hazy images $I = \{i^{(1)}, i^{(2)}, \dots, i^{(m)}\}$ and corresponding ground truth images $J = \{j^{(1)}, j^{(2)}, \dots, j^{(m)}\}$;

Initialize δ by uniform distribution $U(-\epsilon, \epsilon)$ and δ is clipped by Equation (6);

for k steps **do**

Calculate the attack loss L_G ;

Update δ by Equations (4), (5) and (6).

end for

Generate the attacked prediction J_p^δ by Equation (2);

Calculate the adversarial training loss L_{def}^G ;

Update parameters θ for Γ_θ :

$$\theta = \theta - lr \times \nabla_\theta L_{def}^G. \quad (16)$$

end for

Based on the above two factors, we conduct the research on adversarial training defense [5] to protect the dehazing networks.

From the perspective of defense, the adversarial training process against the five attack methods can be divided into two categories. The first way is to use the original dehazed image J_p to reduce the distance between the J_p^δ and J_p . Therefore, the adversarial training process needs to use the pre-trained dehazing model as a teacher network to produce the original dehazed image J_p . The second way is to use clear image J to reduce the distance between J_p^δ and J .

For the two defense ways, we chose L_P and L_J to design the corresponding adversarial training process, as shown in Algorithm 1 and Algorithm 2. Other attack methods can use Algorithm 1 and Algorithm 2 for their own adversarial training processes.

The overall losses of the corresponding defense methods for L_P and L_G are L_{def}^P (Equation (19)) and L_{def}^G (Equation (20)), respectively. The adversarial training defense is a min-max (mm) game, as follows,

$$L_{mm}^P = \min_{\theta} \mathbb{R}(J_p^{\delta}, J_p^T) \max_{\|\delta\|_{\infty} \leq \epsilon} \mathbb{R}(J_p^{\delta}, J_p^T), \quad (17)$$

$$L_{mm}^G = \min_{\theta} \mathbb{R}(J_p^{\delta}, J) \max_{\|\delta\|_{\infty} \leq \epsilon} \mathbb{R}(J_p^{\delta}, J). \quad (18)$$

Since the parameters θ of dehazing network Γ_{θ} will be changed during the adversarial training process, the Teacher network Γ_{θ}^T with fixed parameters is adopted to obtain predicted dehazed image J_p^T ($J_p^T = \Gamma_{\theta}^T(I)$) for L_{def}^P . To insure the dehazing network can still handle the hazy images I that have not been attacked, the basic image restoration loss function should be adopted to the final defense loss

$$L_{def}^P = \mathbb{R}(\Gamma_{\theta}(I), J) + \lambda L_{mm}^P, \quad (19)$$

$$L_{def}^G = \mathbb{R}(\Gamma_{\theta}(I), J) + \lambda L_{mm}^G, \quad (20)$$

where λ is the balance factor for the original image restoration loss function and adversarial defense loss function. Adversarial training defense process do not need to start from scratch. The parameters can be initialized by the well-trained network, and fine-tuned on the adversarial examples. Details about adversarial training defense L_{def}^P are shown in Figure 1 (c).

IV. EXPERIMENTS

The experiments contain three parts, which are attack results, defense results and discussions in Subsections IV-A, IV-B and IV-C, respectively. Figure 5 shows instances of the original hazy and corresponding clear images, respectively. The attack and defense codes are provided. It takes about 8 months to conduct the experiments of this paper under the condition of using a single NVIDIA V100 32G GPU.

A. Experiments on Attack

1) *Settings on Attack*: To show the attack results on different datasets with different scales, the experiments are conducted on six different datasets: ITS (indoor) and OTS (outdoor) from RESIDE [50], I-HAZE [51], O-HAZE [52], D-Hazy [53], 4K [11] and Foggy-City [54], [55]. The details about these datasets can be found in corresponding papers.

The batch size is the same for all the baseline dehazing networks trained on the same dataset, that is 8 for ITS/OTS/4K and 4 for D-Hazy/I-HAZE/O-HAZE/Foggy-City. The image size for ITS/OTS/4K/I-HAZE/O-HAZE, D-Hazy and Foggy-City are 256×256 , 480×640 and 256×512 , respectively. We choose the widely used metric PSNR and SSIM [47] for the evaluation, which are consistent with our attack loss functions. Lower PSNR and SSIM value stand for worse dehazing results, while represent better attack performance.

To ensure that the attack results are reliable, we choose the widely cited papers (dehazing algorithms) that are published on well-known conferences as baselines. The baselines methods are AODNet [6], DM2FNet [7], GCANet [20], MSBDN [8], FFANet [9], GridDehazeNet [10] and 4KDehazing [11], respectively.

The choice of parameters is theoretically infinite. For the attack experiments, the ϵ is chosen from $\{0, 2, 4, 6, 8\}$, and α is set to 2. Both ϵ and α are divided by 255. The $\epsilon = 0$ means no attack. The attack iteration steps are 10. Initialized values of δ for attacking and the noise for noise attack A_N are both sampled from uniform distribution $U(-\epsilon, \epsilon)$. The attack methods contain L_P^{MSE} , A_N , L_M^{MSE} , L_G^{MSE} , L_I^{MSE} and L_P^{SSIM} , respectively. The attack process is to maximize these loss functions (except noise attack A_N). It is worth noting that the *mask* in L_M (L_M^{MSE}) has three channels obtained by copying a single channel. The μ used to obtain the *mask* is calculated on the whole image (channel average) as shown in Equation (9). Any position (m, n) in the hazy image I is either be attacked or not attacked. Therefore, *mask*(m, n) equals 1 when any channel in position (m, n) satisfied $I(m, n) - J_p(m, n) > \mu$.

2) *Results on Attack*: Here, quantitative and visual evaluations of the attack results are given. Furthermore, the corresponding conclusions and analyses are provided.

Quantitative Results: Table I shows the attack results obtained by L_P^{MSE} , A_N , L_M^{MSE} , L_G^{MSE} , L_I^{MSE} and L_P^{SSIM} on various datasets. The results summarized from Table I are as follows.

- L_P^{MSE} : The attacker can use predicted dehazed images obtained by dehazing networks as pseudo labels to attack the dehazing networks. As ϵ increases from 2 to 8, the attack performance gradually increases.
- A_N : The performance of general noise attack A_N is obvious lower than other attack methods that use gradient information, which verifies that the proposed first order gradient based attack methods are much stronger than general noise.
- L_M^{MSE} : The quantitative results obtained by L_M^{MSE} prove that the partial attack is reliable, that is we do not need to attack the whole image.
- L_G^{MSE} : The metric values of L_G^{MSE} and L_P^{MSE} are quite close, which indicates that the attacker is not required to have the ground truth clear images for attacking process.
- L_I^{MSE} : The results show that L_I^{MSE} is a promising attack method, which also allows the attacker to perform the attacking process without paired data.
- L_P^{SSIM} : The results obtained by L_P^{MSE} has demonstrated that first order attack can reduce the dehazing performance by MSE loss. The usage of L_P^{SSIM} can achieve relative lower SSIM, which proves the SSIM loss can also be used for first order attack.

Visual Results: The analysis of visual results on various datasets with different loss functions are as follows.

- L_P^{MSE} : The visual results obtained by the dehazing networks after different level (ϵ) attacks on Foggy-City are shown in Figure 3. It can be seen that with increase of ϵ , the visual dehazing results tend to be more unsatisfactory.

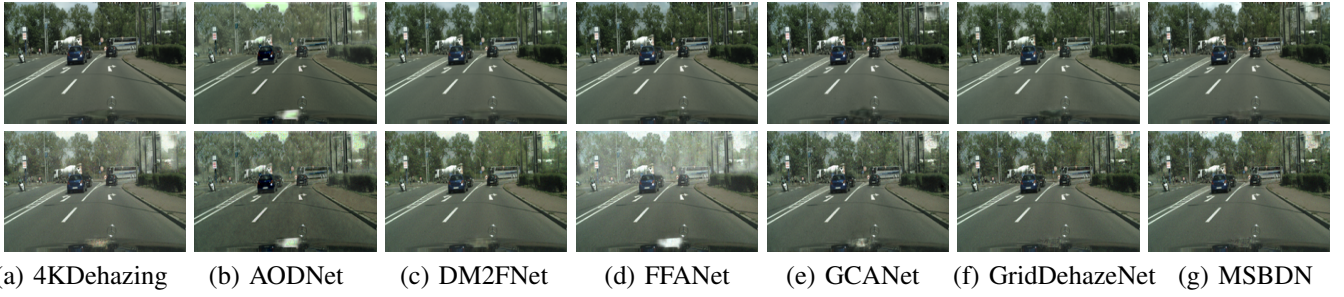


Fig. 2. Dehazing visual results obtained by A_N . The ϵ of top row and bottom row are 0 and 8, respectively. Images are from Foggy-City.

- A_N : The visual results in Figure 2 show the original dehazed outputs ($\epsilon = 0$) and the predicted attacked outputs ($\epsilon = 8$). Although ϵ is set to 8, the texture and structure of attacked outputs are still consistent with the original dehazed outputs.
- L_M^{MSE} : Figure 6 compares the visual performance between a mask attack and an non-mask attack method. The mask attack can achieve similar effects as the non-mask attack, which shows that the attacker can partially attack the input hazy image, rather than the whole image.
- L_G^{MSE} : The attacked dehazed results J_p^δ (under attack loss L_G^{MSE}) are shown in Figure 7. The attack visual performances of Figure 7 are quite close to the attack visual results (under attack loss L_P^{MSE}) shown in Figure 3, which demonstrates that taking predicted dehazed images (J_p) as pseudo labels is a promising way to attack (attack loss L_P^{MSE}) the dehazing networks.
- L_I^{MSE} : The attacked hazy images $I^\delta = I + \delta$ and predicted attacked dehazed images J_p^δ shown in Figure 4 are quite close from the perspective of visual perception when $\epsilon > 0$. This phenomenon illustrates that the identity attack loss L_I^{MSE} can preserve the haze inside the hazy scenes.
- L_P^{SSIM} : Figure 8 shows the outdoor attack results obtained by attack loss L_P^{SSIM} . With the increase of ϵ , the visual quality of dehazed images all decreases, which shows the effectiveness of the attack method based on SSIM loss.

Conclusions and Analyses: From the quantitative results and visual results, two main conclusions can be summarized. The reasons for the conclusions are intuitive and simple, as follows.

- The negative impact caused by the perturbation δ on the dehazing model is significantly stronger than that of regular noise. The reason is that the δ is generated by adjusting the distance between J_p^δ and X . Moreover, the generation process of the δ utilizes the specific dehazing model. However, these two factors are not available in regular noise. Therefore, the attack effect of δ is stronger than regular noise.
- Using the predicted image J_p as pseudo-label can attack the dehazing model successfully, although it is slightly less effective than using the ground-truth haze-free image J as the guidance information. The reason is that the J_p obtained by the well-trained dehazing model is close to J . For the attacker, increasing the distance between J_p^δ and

J_p is approximately equivalent to increasing the distance between J_p^δ and J .

B. Experiments on Defense

1) *Settings on Defense:* The λ in Equations (19) and (20) are set to 1. Other settings for dehazing networks are consistent with the Subsection IV-A1. The epochs for defense training is set to 40 and ϵ is fixed as 8 (maximum attack degree). Since the adversarial examples are generated dynamically, the adversarial defense training time under each epoch is almost k (iteration steps for generating δ) times of the original training time. The defense training strategy is verified by using 4KDehazing, AODNet, GCANet, GridDehazeNet and MSBDN.

2) *Results on Defense:* Here we show the attack results after adversarial defense training both quantitatively and visually. In addition, the summaries and analyses of the defense results are also provided.

Quantitative Results: Table II shows the quantitative attack results before and after defense training. The results summarized from Table II are as follows.

- The adversarial defense training is quite effective for protecting the dehazing networks and the dehazing performance after defense training are obvious better (higher PSNR and SSIM) than that before defense training. Meanwhile, with the increases of ϵ , the PSNR and SSIM that after defense training decrease slowly than that before defense training.
- “Method: TP” (trained by L_{def}^P) and “Method: TG” (trained by L_{def}^G) in Table II show the dehazing results on original hazy examples I (without attack). It can be seen that adversarial defense training will slightly reduce the dehazing performance on original hazy examples in most cases.

Visual Results: Figure 10 shows the visual attack results before and after defense training. It can be seen that the attack results after defense training are more visually pleasing than those before defense training.

Conclusions and Analyses: The main conclusion summarized from the quantitative and visual results is that the adversarial defense training can protect the dehazing networks, but it can not “totally” eliminate the negative effects caused by attacker. The reason is that the dehazing model have seen the adversarial examples during defense training, so its robustness

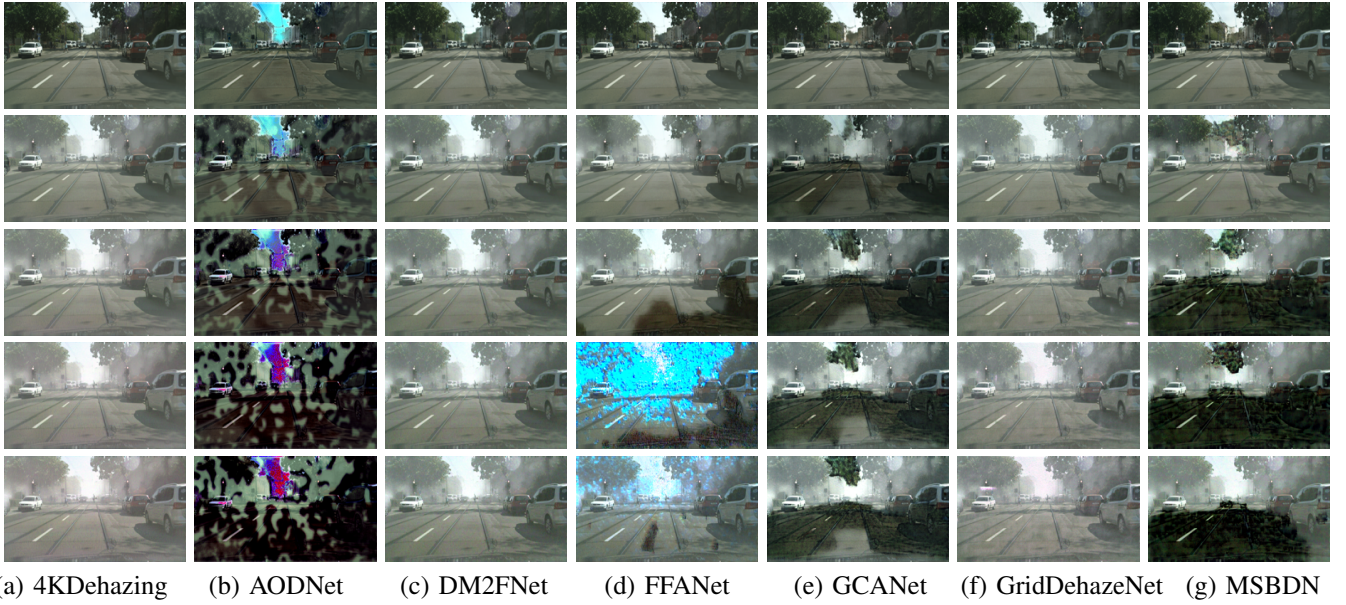


Fig. 3. Image dehazing visual results obtained by different dehazing algorithms under attack loss L_P^{MSE} . The ϵ of each row from up to down are 0, 2, 4, 6 and 8, respectively. Images are from Foggy-City.

is improved. However, the attacker is still able to obtain the gradient information of the dehazing model that has performed the defense training [14]. Therefore, the attacker can still suboptimally find the weaknesses of the dehazing model. The distribution of original hazy images is denoted as P_I , the distribution of original hazy images and hazy images that after adding adversarial perturbations is denoted as P_{I+I^δ} , and distribution of clear images J is P_J . The regular training process is to learn the mapping from P_I to P_J , while the defense training process learns the mapping from P_{I+I^δ} to P_J . The goals of defense training and regular training are different. This phenomenon is consistent with the classification task [5], which leads to the need for a balance between the robustness and the performance of the model [56]. Therefore, the performance of the dehazing model that after defense training on the original hazy image will be slightly worse.

C. Discussions and Verifications

1) *The Convergence of Adversarial Training:* To verify the stability during the training process of adversarial defense training, the loss values on Foggy-City are recorded and averaged every 500 iterations. The corresponding loss curves are plotted in Figure 9. It can be seen from Figure 9 that the loss functions are basically convergent. It is worth noting that the adversarial training process on our dehazing task is a min-max game, rather than a single minimization training. It is reasonable that the min-max process has oscillations. In order to avoid the “over-fitting” on defense training, we stop the defense training when the quantitative metrics (PSNR and SSIM) are stable. Therefore, the loss function curves do not fully converge to a nearly flat straight line.

2) *The Evaluation of Hazy Images after Attack:* The hazy image after attack is $I^\delta = I + \delta$, which is different from the original hazy image I . The attacker aims at generating a subtle perturbation δ . Therefore, we need to evaluate the difference

between I^δ and I to analyze how the attacker affects the hazy input. Figure 11 and Figure 12 show two important results on D-Hazy dataset: the metrics between I^δ and I that are denoted as $I^\delta - \epsilon$, and the metrics between J_p^δ and J that are denoted as $J_p^\delta - \epsilon$. Figure 14 shows the corresponding visual results of I^δ and J_p^δ . As we can see, the negative effects of adversarial attack on hazy images are lower than that on predicted dehazed images.

Mean subtracted contrast normalized (MSCN) [57] coefficient is a well-known concept in natural scene statistics. Kherchouche et al. [29] argue that the histograms of MSCN coefficients of adversarial examples are visually different from the original image. More specifically, the histograms of original images are Gaussian-like, while the histograms of adversarial examples are obvious not. The observation of Kherchouche’s experiments are conducted on image recognition task. However, in our dehazing task, we find that the histograms of adversarial examples are still obeying the Gaussian-like distributions as shown in Figure 13.

3) *Multi-step Attack and Defense:* The attacker takes an iteration-based strategy to attack the dehazing networks. The iteration step is k . To investigate how k affects the attack and defense performance, we set k to different values and calculate the corresponding dehazing results.

Table III shows the attack results obtained by attack loss L_P^{MSE} when $k \in \{1, 2, 3, 5, 10, 15, 20, 25, 30\}$. The results in Table III indicate that with the increases of k , the attack performance increases in most cases. The attack effect does not increase significantly when $k > 10$. The possible reason for this phenomenon is that the value of ϵ is limited to 4. Therefore, the attack effect of an attacker who modifies the pixel value within the range $(-4, 4)$ will not continue to grow rapidly.

For adversarial defense training stage, k is randomly selected from $\{20, 25, 30\}$ in each iteration. The attack results

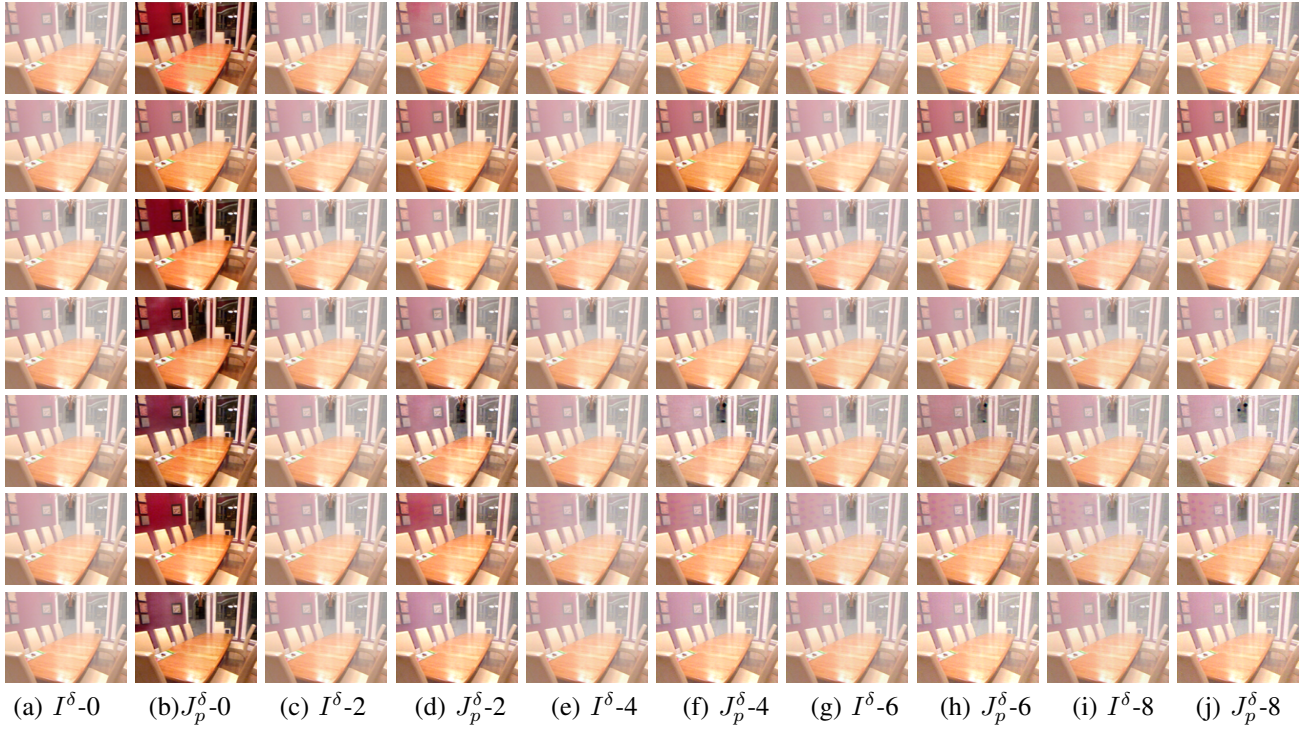


Fig. 4. Attack visual results obtained by L_I^{MSE} . The attacked hazy image and corresponding prediction (dehazed image) are denoted as $I^\delta - \epsilon$ and $J_p^\delta - \epsilon$, respectively. $\epsilon \in \{0, 2, 4, 6, 8\}$. The algorithms of each row from up to down are 4KDehazing, AODNet, DM2FNet, FFANet, GCANet, GridDehazeNet and MSBDN, respectively. Images are from ITS.

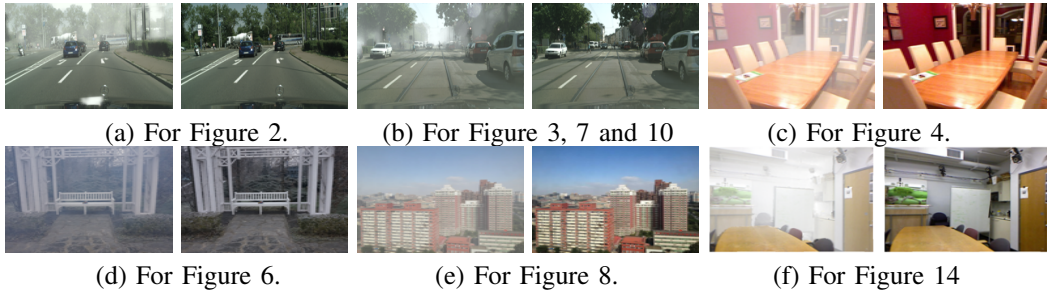


Fig. 5. The original hazy images I and corresponding clear images J .

before and after defense training are shown in Table IV, which can achieve the same conclusions as the analysis in Subsection IV-B2. The results indicate that adversarial defense training with multi-step attack is effective when the attacker adopts different attack iterations (k) in most cases.

V. CONCLUSION

In this paper, we try to explore and define a new research problem, which is called AADN. A first order attack algorithm is found to be powerful to attack the dehazing networks, which will lead to the performance reduction of the dehazing task. Meanwhile, several attack forms are proposed and verified for different attack purposes. Finally, we explore the effectiveness of adversarial defense training to protect the vulnerable dehazing networks. We have investigated the fundamental problems of attacking dehazing networks. Since we must control the size of this paper, more attack and defense methods on the issue of the security of dehazing network will be studied in the future.

REFERENCES

- [1] H. Liu, Z. Wu, L. Li, S. Salehkalibar, J. Chen, and K. Wang, "Towards multi-domain single image dehazing via test-time training," in *Proceedings of the IEEE/CVF Conference on Computer Vision and Pattern Recognition*, 2022, pp. 5831–5840.
- [2] Y. Yang, C. Wang, R. Liu, L. Zhang, X. Guo, and D. Tao, "Self-augmented unpaired image dehazing via density and depth decomposition," in *Proceedings of the IEEE/CVF Conference on Computer Vision and Pattern Recognition*, 2022, pp. 2037–2046.
- [3] M. Hong, Y. Xie, C. Li, and Y. Qu, "Distilling image dehazing with heterogeneous task imitation," in *Proceedings of the IEEE/CVF Conference on Computer Vision and Pattern Recognition*, 2020, pp. 3462–3471.
- [4] J. Gui, X. Cong, Y. Cao, W. Ren, J. Zhang, J. Zhang, and D. Tao, "A comprehensive survey on image dehazing based on deep learning," in *Proceedings of the Thirtieth International Joint Conference on Artificial Intelligence*, Z.-H. Zhou, Ed. International Joint Conferences on Artificial Intelligence Organization, 8 2021, pp. 4426–4433, survey Track. [Online]. Available: <https://doi.org/10.24963/ijcai.2021/604>
- [5] A. Madry, A. Makelov, L. Schmidt, D. Tsipras, and A. Vladu, "Towards deep learning models resistant to adversarial attacks," *arXiv preprint arXiv:1706.06083*, 2017.
- [6] B. Li, X. Peng, Z. Wang, J. Xu, and D. Feng, "Aod-net: All-in-one

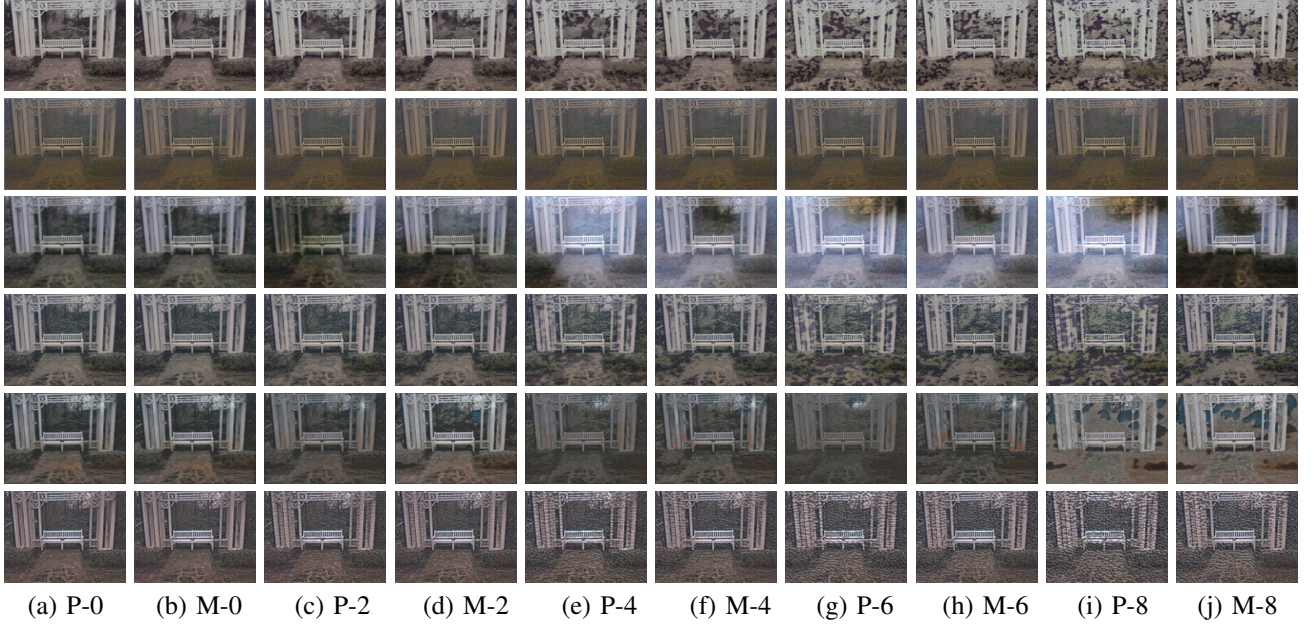


Fig. 6. Attack visual results obtained by L_P^{MSE} and L_M^{MSE} , which are represented by P and M , respectively. The $P - \epsilon$ and $M - \epsilon$ denote the results when $\epsilon \in \{0, 2, 4, 6, 8\}$. The algorithms of each row from up to down are 4KDehazing, AODNet, DM2FNet, FFANet, GCANet, and GridDehazeNet, respectively. Images are from O-HAZE.

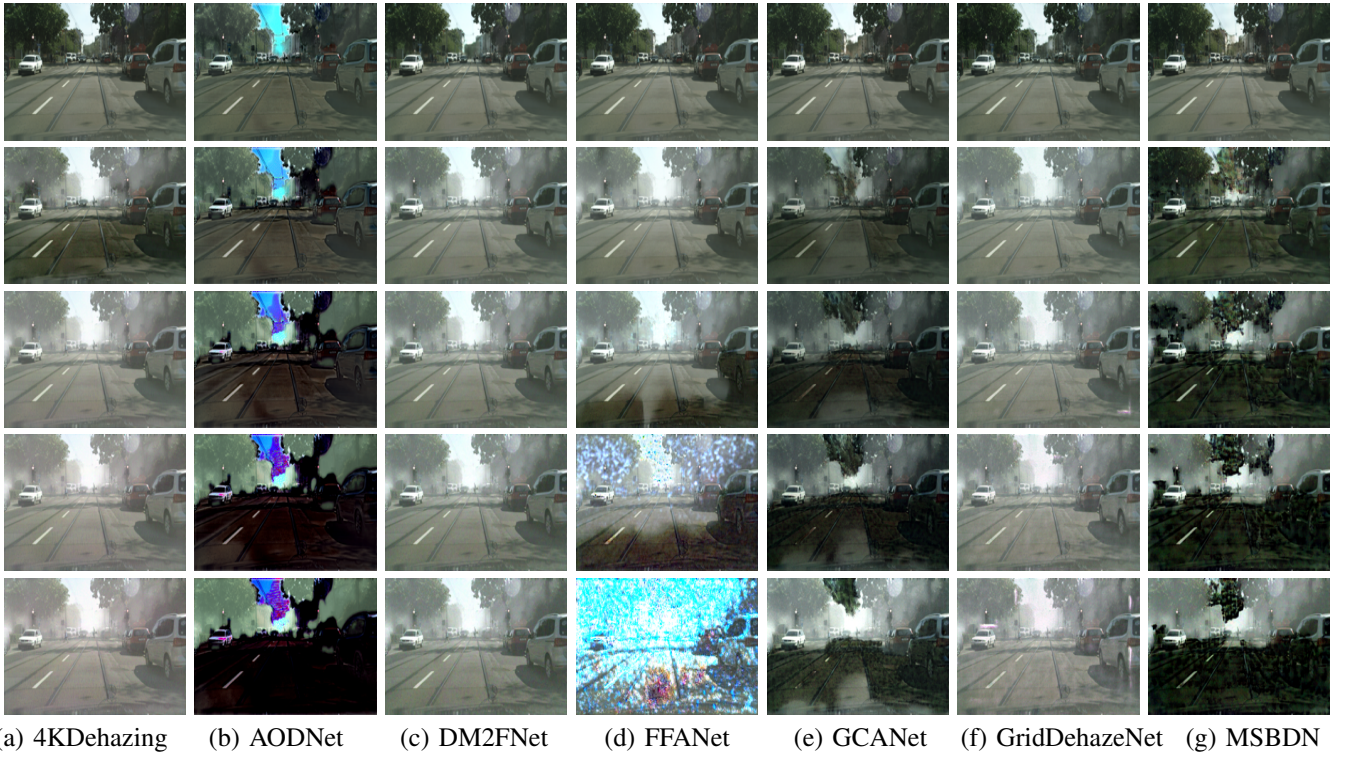


Fig. 7. Attack visual results obtained by attack loss L_G^{MSE} . The ϵ of each row from up to down are 0, 2, 4, 6 and 8, respectively. Images are from Foggy-City.

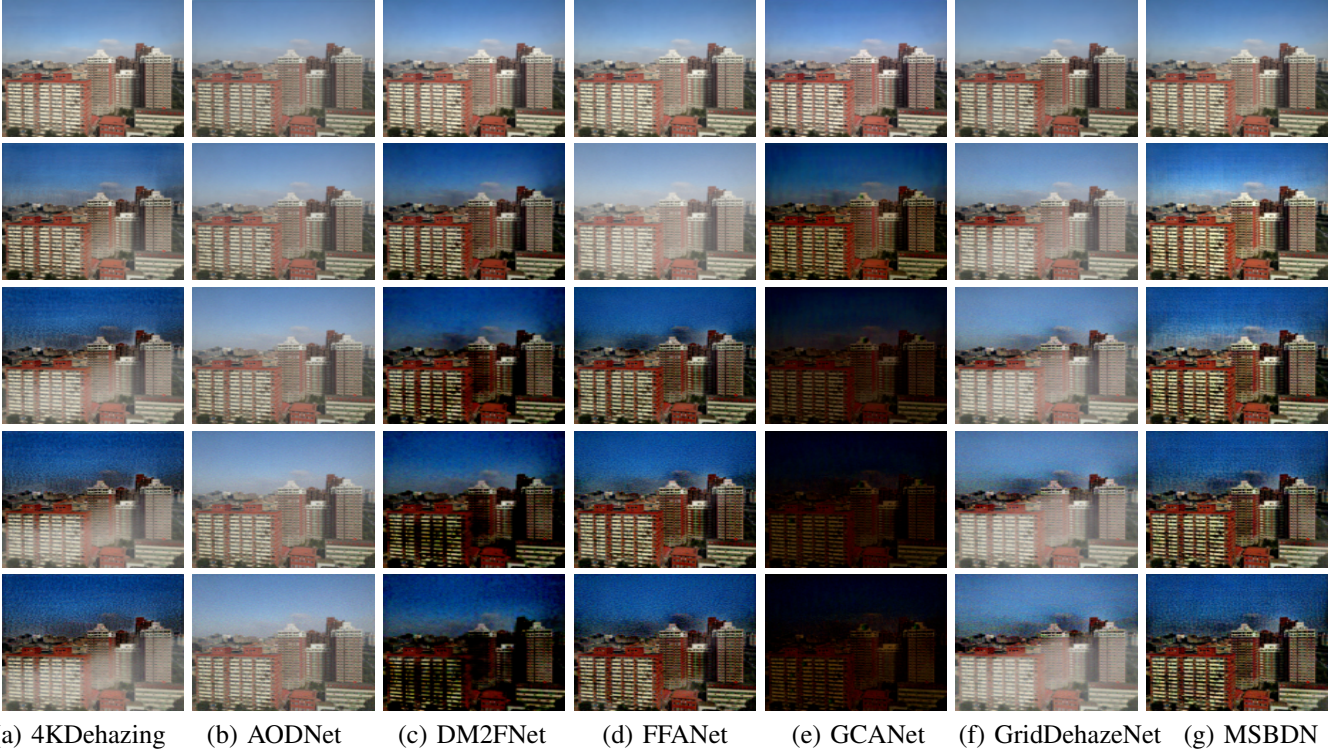


Fig. 8. Image dehazing visual results obtained by different dehazing algorithms under attack loss L_P^{SSIM} . The ϵ of each row from up to down are 0, 2, 4, 6 and 8, respectively. Images are from OTS.

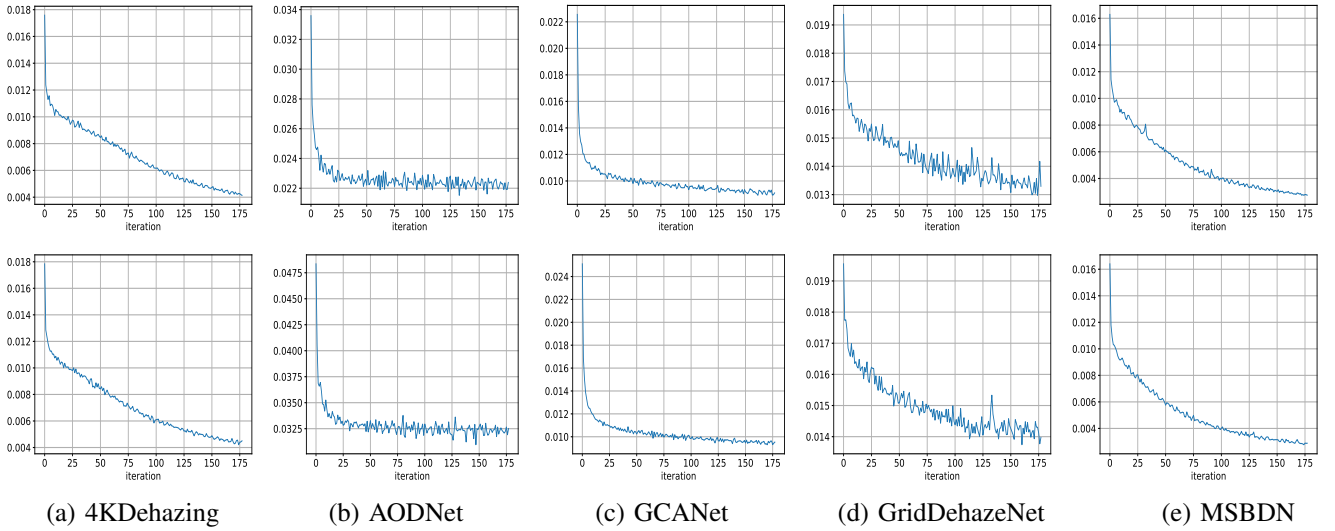


Fig. 9. The convergence of different dehazing algorithms during adversarial training on Foggy-City. The top row is L_{def}^P , and the second row is L_{def}^G . The horizontal axis indicates the number of iterations (the average of 500 iterations). The vertical axis represents the corresponding loss value. The min-max defense training process is stopped when the quantitative metrics are stable to avoid overfitting. Therefore, some loss curves may not converge to a nearly flat straight line.

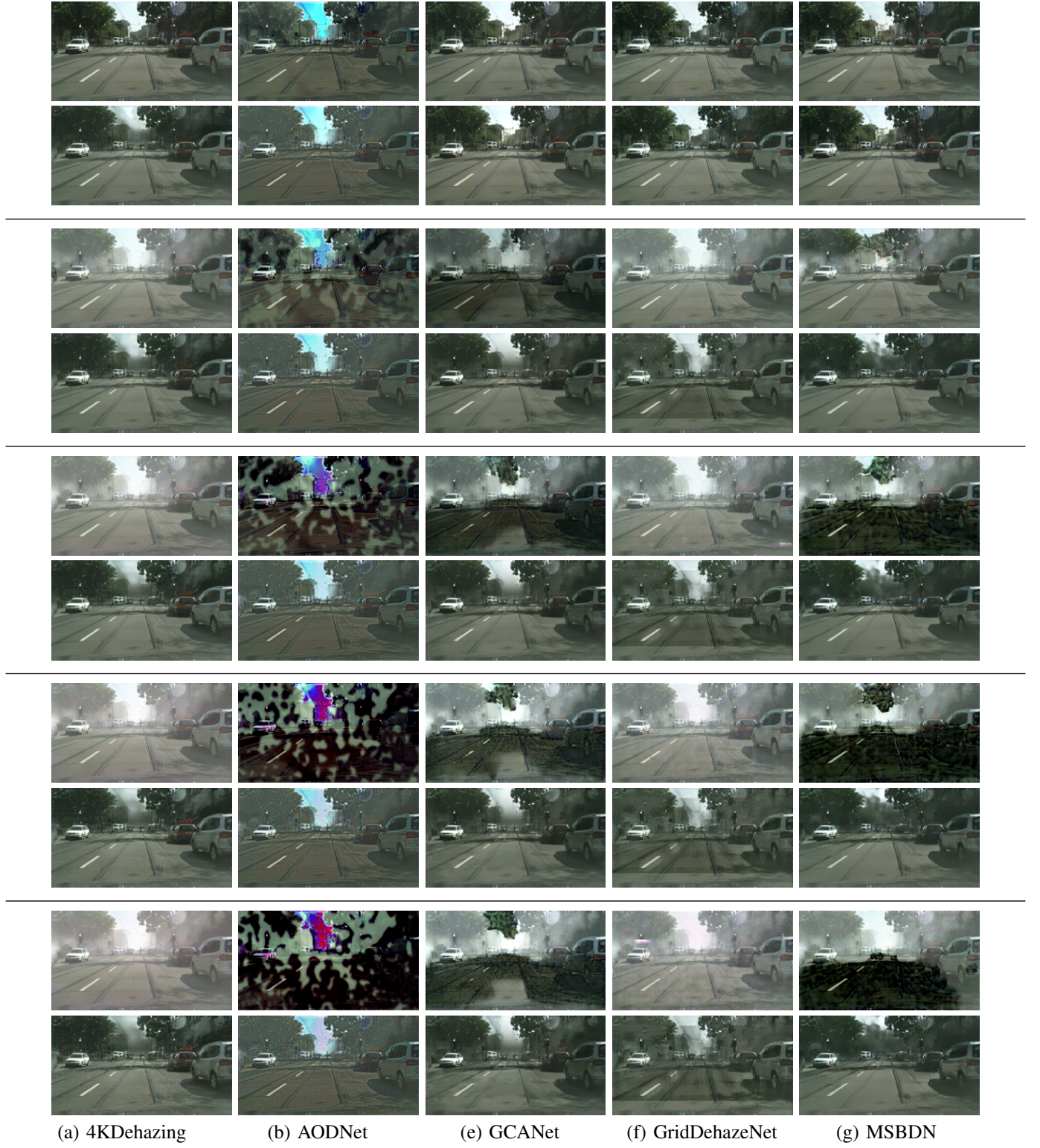


Fig. 10. Image dehazing results obtained by different dehazing algorithms under attack loss L_P^{MSE} before and after defense training. Every two rows of images are in a group. The above images of each group are the results of direct attack (without defense training), and the bottom images are the results of attack after defense training. The ϵ of two rows from up to down are 0, 2, 4, 6 and 8, respectively. Images are from Foggy-City.

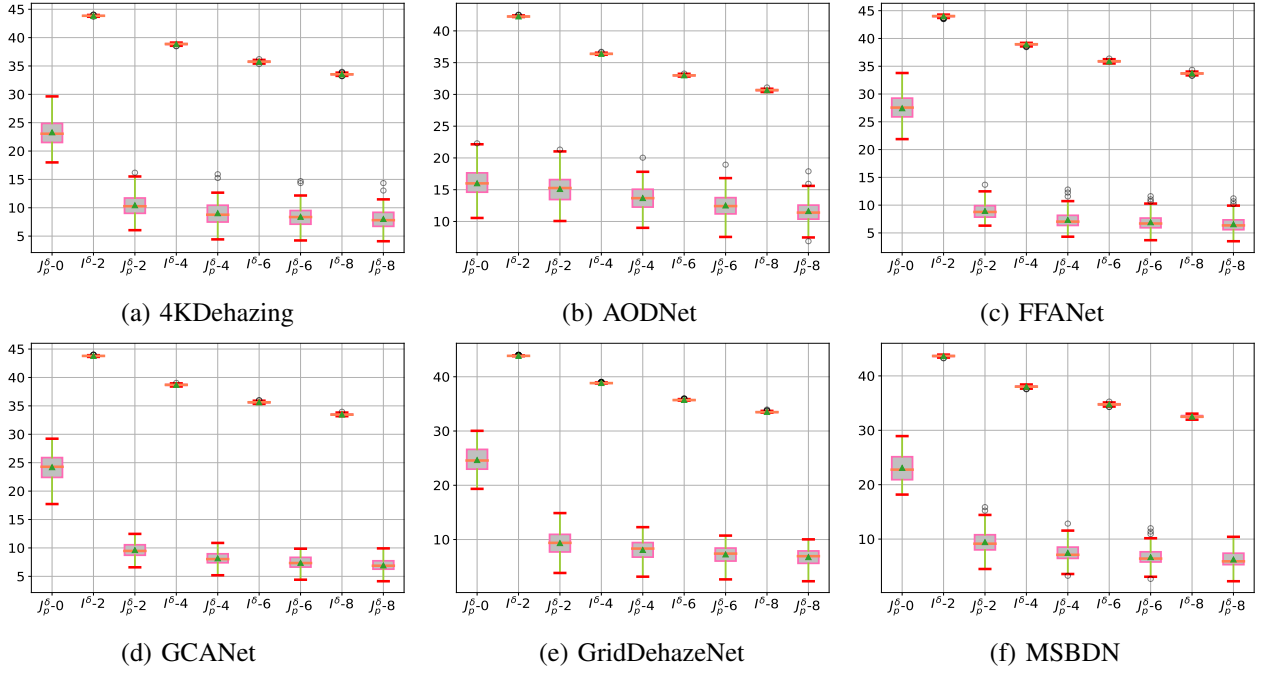


Fig. 11. The PSNR values under attack loss L_P^{MSE} on D-Hazy. The horizontal coordinates $I^\delta - \epsilon$, $J_p^\delta - \epsilon$ denote the PSNR between I^δ and I , the PSNR between J_p^δ and J , respectively. The ϵ is in $\{0, 2, 4, 6, 8\}$.

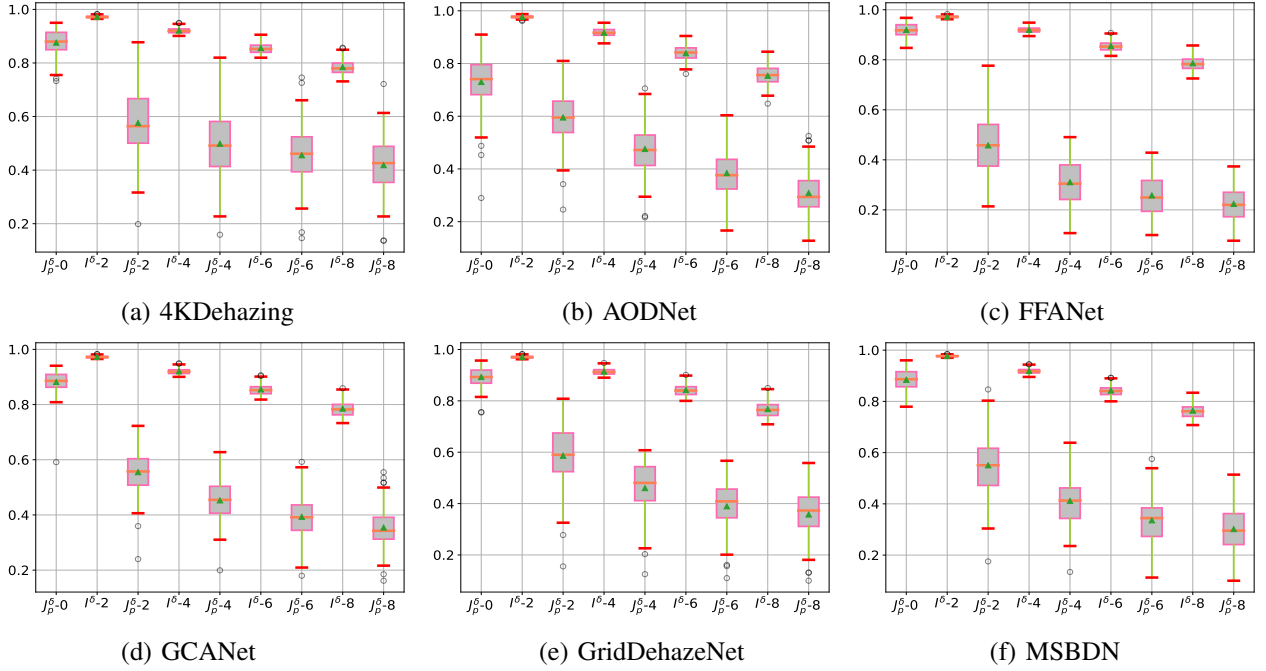


Fig. 12. The SSIM values under attack loss L_P^{MSE} on D-Hazy. The horizontal coordinates $I^\delta - \epsilon$, $J_p^\delta - \epsilon$ denote the SSIM between I^δ and I , the SSIM between J_p^δ and J , respectively. The ϵ is in $\{0, 2, 4, 6, 8\}$.

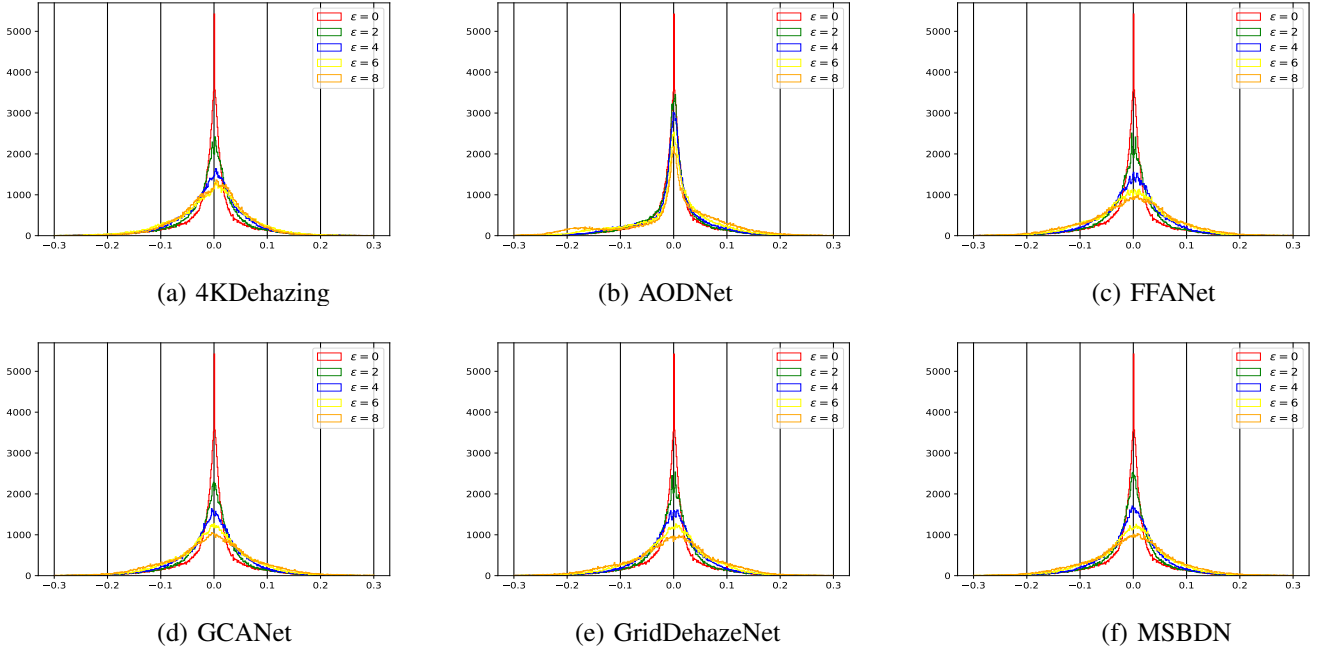


Fig. 13. The histograms of MSCN coefficient on Foggy-City under attack loss L_P^{MSE} .

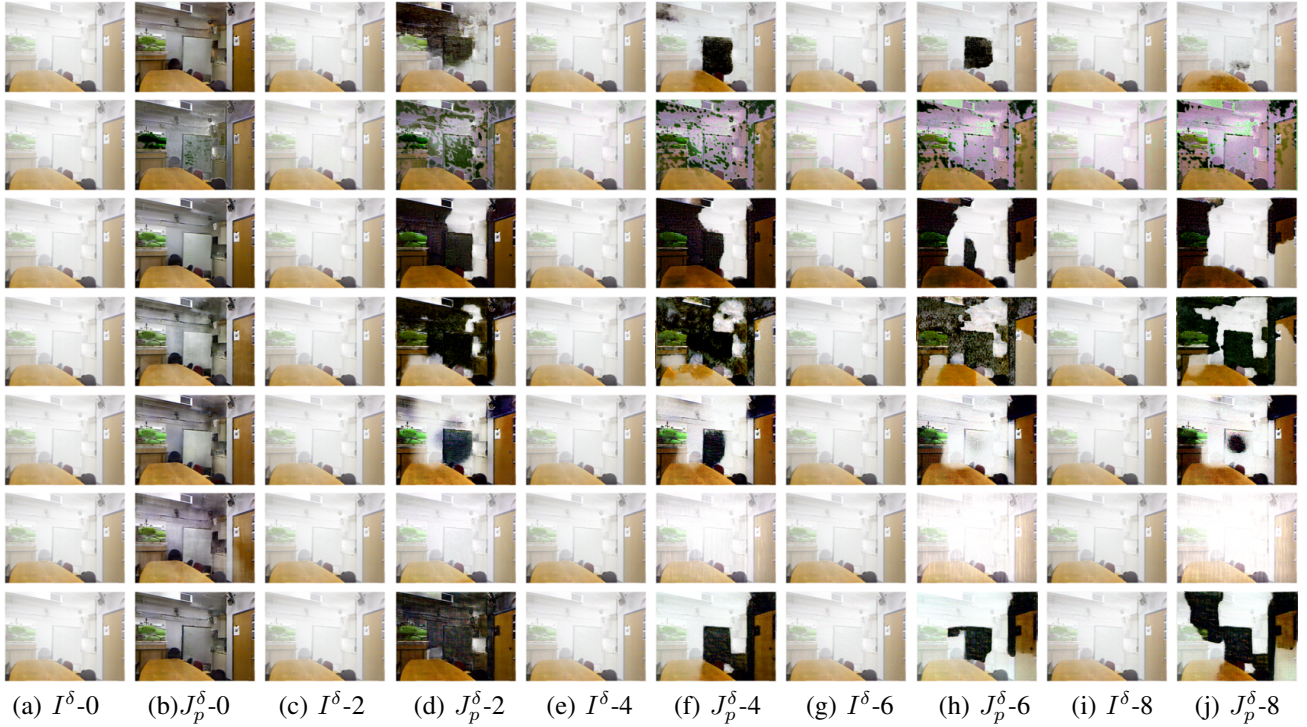


Fig. 14. Attack visual results (under attack loss L_P^{MSE}) between $I^\delta - \epsilon$ and $J_p^\delta - \epsilon$, respectively. The ϵ is in $\{0, 2, 4, 6, 8\}$. The algorithms of each row from up to down are 4KDehazing, AODNet, DM2FNet, FFANet, GCANet, GridDehazeNet and MSBDN, respectively. Images are from D-Hazy.

- dehazing network,” in *Proceedings of the IEEE international conference on computer vision*, 2017, pp. 4770–4778.
- [7] Z. Deng, L. Zhu, X. Hu, C.-W. Fu, X. Xu, Q. Zhang, J. Qin, and P.-A. Heng, “Deep multi-model fusion for single-image dehazing,” in *Proceedings of the IEEE/CVF international conference on computer vision*, 2019, pp. 2453–2462.
 - [8] H. Dong, J. Pan, L. Xiang, Z. Hu, X. Zhang, F. Wang, and M.-H. Yang, “Multi-scale boosted dehazing network with dense feature fusion,” in *Proceedings of the IEEE/CVF conference on computer vision and pattern recognition*, 2020, pp. 2157–2167.
 - [9] X. Qin, Z. Wang, Y. Bai, X. Xie, and H. Jia, “Ffa-net: Feature fusion attention network for single image dehazing,” in *Proceedings of the AAAI Conference on Artificial Intelligence*, vol. 34, no. 07, 2020, pp. 11 908–11 915.
 - [10] X. Liu, Y. Ma, Z. Shi, and J. Chen, “Griddehazenet: Attention-based multi-scale network for image dehazing,” in *Proceedings of the IEEE/CVF international conference on computer vision*, 2019, pp. 7314–7323.
 - [11] Z. Zheng, W. Ren, X. Cao, X. Hu, T. Wang, F. Song, and X. Jia, “Ultra-high-definition image dehazing via multi-guided bilateral learning,” in *2021 IEEE/CVF Conference on Computer Vision and Pattern Recognition (CVPR)*. IEEE, 2021, pp. 16 180–16 189.
 - [12] X. Yuan, P. He, Q. Zhu, and X. Li, “Adversarial examples: Attacks and defenses for deep learning,” *IEEE transactions on neural networks and learning systems*, vol. 30, no. 9, pp. 2805–2824, 2019.
 - [13] K. Ren, T. Zheng, Z. Qin, and X. Liu, “Adversarial attacks and defenses in deep learning,” *Engineering*, vol. 6, no. 3, pp. 346–360, 2020.
 - [14] N. Akhtar, A. Mian, N. Kardan, and M. Shah, “Advances in adversarial attacks and defenses in computer vision: A survey,” *IEEE Access*, vol. 9, pp. 155 161–155 196, 2021.
 - [15] A. Kherchouche, S. A. Fezza, and W. Hamidouche, “Detect and defense against adversarial examples in deep learning using natural scene statistics and adaptive denoising,” *Neural Computing and Applications*, pp. 1–16, 2021.
 - [16] X. Zhang, R. Jiang, T. Wang, and W. Luo, “Single image dehazing via dual-path recurrent network,” *IEEE Transactions on Image Processing*, vol. 30, pp. 5211–5222, 2021.
 - [17] Q. Deng, Z. Huang, C.-C. Tsai, and C.-W. Lin, “Hardgan: A haze-aware representation distillation gan for single image dehazing,” in *European Conference on Computer Vision*. Springer, 2020, pp. 722–738.
 - [18] H. Li, J. Li, D. Zhao, and L. Xu, “Dehazeflow: Multi-scale conditional flow network for single image dehazing,” in *Proceedings of the 29th ACM International Conference on Multimedia*, 2021, pp. 2577–2585.
 - [19] Y. Li, Y. Chang, Y. Gao, C. Yu, and L. Yan, “Physically disentangled intra-and inter-domain adaptation for varicolored haze removal,” in *Proceedings of the IEEE/CVF Conference on Computer Vision and Pattern Recognition*, 2022, pp. 5841–5850.
 - [20] D. Chen, M. He, Q. Fan, J. Liao, L. Zhang, D. Hou, L. Yuan, and G. Hua, “Gated context aggregation network for image dehazing and deraining,” in *IEEE winter conference on applications of computer vision*. IEEE, 2019, pp. 1375–1383.
 - [21] H. Wu, Y. Qu, S. Lin, J. Zhou, R. Qiao, Z. Zhang, Y. Xie, and L. Ma, “Contrastive learning for compact single image dehazing,” in *Proceedings of the IEEE/CVF Conference on Computer Vision and Pattern Recognition*, 2021, pp. 10 551–10 560.
 - [22] P. Shyam, K.-J. Yoon, and K.-S. Kim, “Towards domain invariant single image dehazing,” in *Proceedings of the AAAI Conference on Artificial Intelligence*, vol. 35, no. 11, 2021, pp. 9657–9665.
 - [23] P. Li, J. Tian, Y. Tang, G. Wang, and C. Wu, “Deep retinex network for single image dehazing,” *IEEE Transactions on Image Processing*, vol. 30, pp. 1100–1115, 2020.
 - [24] Z. Chen, Y. Wang, Y. Yang, and D. Liu, “Psd: Principled synthetic-to-real dehazing guided by physical priors,” in *Proceedings of the IEEE/CVF conference on computer vision and pattern recognition*, 2021, pp. 7180–7189.
 - [25] C.-L. Guo, Q. Yan, S. Anwar, R. Cong, W. Ren, and C. Li, “Image dehazing transformer with transmission-aware 3d position embedding,” in *Proceedings of the IEEE/CVF Conference on Computer Vision and Pattern Recognition*, 2022, pp. 5812–5820.
 - [26] F. Tramer, N. Carlini, W. Brendel, and A. Madry, “On adaptive attacks to adversarial example defenses,” *Advances in Neural Information Processing Systems*, vol. 33, pp. 1633–1645, 2020.
 - [27] A. Athalye, N. Carlini, and D. Wagner, “Obfuscated gradients give a false sense of security: Circumventing defenses to adversarial examples,” in *International conference on machine learning*. PMLR, 2018, pp. 274–283.
 - [28] J. Uesato, B. O’donoghue, P. Kohli, and A. Oord, “Adversarial risk and the dangers of evaluating against weak attacks,” in *International Conference on Machine Learning*. PMLR, 2018, pp. 5025–5034.
 - [29] A. Kherchouche, S. A. Fezza, W. Hamidouche, and O. Déforges, “Detection of adversarial examples in deep neural networks with natural scene statistics,” in *2020 International Joint Conference on Neural Networks*. IEEE, 2020, pp. 1–7.
 - [30] A. Chakraborty, M. Alam, V. Dey, A. Chattopadhyay, and D. Mukhopadhyay, “Adversarial attacks and defenses: A survey,” *arXiv preprint arXiv:1810.00069*, 2018.
 - [31] N. Carlini and D. Wagner, “Towards evaluating the robustness of neural networks,” in *2017 IEEE Symposium on Security and Privacy (SP)*. IEEE, 2017, pp. 39–57.
 - [32] Y. Deldjoo, T. D. Noia, and F. A. Merra, “A survey on adversarial recommender systems: from attack/defense strategies to generative adversarial networks,” *ACM Computing Surveys (CSUR)*, vol. 54, no. 2, pp. 1–38, 2021.
 - [33] I. J. Goodfellow, J. Shlens, and C. Szegedy, “Explaining and harnessing adversarial examples,” *arXiv preprint arXiv:1412.6572*, 2014.
 - [34] A. Kurakin, I. J. Goodfellow, and S. Bengio, “Adversarial examples in the physical world,” in *Artificial intelligence safety and security*. Chapman and Hall/CRC, 2018, pp. 99–112.
 - [35] Y. Yu, W. Yang, Y.-P. Tan, and A. C. Kot, “Towards robust rain removal against adversarial attacks: A comprehensive benchmark analysis and beyond,” in *Proceedings of the IEEE/CVF Conference on Computer Vision and Pattern Recognition*, 2022, pp. 6013–6022.
 - [36] C. Xie, J. Wang, Z. Zhang, Y. Zhou, L. Xie, and A. Yuille, “Adversarial examples for semantic segmentation and object detection,” in *Proceedings of the IEEE international conference on computer vision*, 2017, pp. 1369–1378.
 - [37] K. K. Nakka and M. Salzmann, “Indirect local attacks for context-aware semantic segmentation networks,” in *European Conference on Computer Vision*. Springer, 2020, pp. 611–628.
 - [38] A. Castillo, M. Escobar, J. C. Pérez, A. Romero, R. Timofte, L. Van Gool, and P. Arbelaez, “Generalized real-world super-resolution through adversarial robustness,” in *Proceedings of the IEEE/CVF International Conference on Computer Vision*, 2021, pp. 1855–1865.
 - [39] A. Mustafa, S. H. Khan, M. Hayat, J. Shen, and L. Shao, “Image super-resolution as a defense against adversarial attacks,” *IEEE Transactions on Image Processing*, vol. 29, pp. 1711–1724, 2019.
 - [40] J.-H. Choi, H. Zhang, J.-H. Kim, C.-J. Hsieh, and J.-S. Lee, “Evaluating robustness of deep image super-resolution against adversarial attacks,” in *Proceedings of the IEEE/CVF International Conference on Computer Vision*, 2019, pp. 303–311.
 - [41] —, “Deep image destruction: A comprehensive study on vulnerability of deep image-to-image models against adversarial attacks,” *arXiv preprint arXiv:2104.15022*, 2021.
 - [42] R. Gao, Q. Guo, F. Juefei-Xu, H. Yu, and W. Feng, “Advhaze: Adversarial haze attack,” *arXiv preprint arXiv:2104.13673*, 2021.
 - [43] S. Kanwal, J. H. Shah, M. A. Khan, M. Nisa, S. Kadry, M. Sharif, M. Yasmin, and M. Maheswari, “Person re-identification using adversarial haze attack and defense: a deep learning framework,” *Computers & Electrical Engineering*, vol. 96, p. 107542, 2021.
 - [44] S. Sun, W. Ren, T. Wang, and X. Cao, “Rethinking image restoration for object detection,” in *Advances in Neural Information Processing Systems*, A. H. Oh, A. Agarwal, D. Belgrave, and K. Cho, Eds., 2022.
 - [45] A. Pal and R. Vidal, “A game theoretic analysis of additive adversarial attacks and defenses,” *Advances in Neural Information Processing Systems*, vol. 33, pp. 1345–1355, 2020.
 - [46] J. Johnson, A. Alahi, and L. Fei-Fei, “Perceptual losses for real-time style transfer and super-resolution,” in *European conference on computer vision*. Springer, 2016, pp. 694–711.
 - [47] Z. Wang, A. C. Bovik, H. R. Sheikh, and E. P. Simoncelli, “Image quality assessment: from error visibility to structural similarity,” *IEEE transactions on image processing*, vol. 13, no. 4, pp. 600–612, 2004.
 - [48] E. J. McCartney, “Optics of the atmosphere: scattering by molecules and particles,” *New York, John Wiley and Sons, Inc.*, 1976.
 - [49] M. Ju, C. Ding, W. Ren, Y. Yang, D. Zhang, and Y. J. Guo, “Ide: Image dehazing and exposure using an enhanced atmospheric scattering model,” *IEEE Transactions on Image Processing*, vol. 30, pp. 2180–2192, 2021.
 - [50] B. Li, W. Ren, D. Fu, D. Tao, D. Feng, W. Zeng, and Z. Wang, “Benchmarking single-image dehazing and beyond,” *IEEE Transactions on Image Processing*, vol. 28, no. 1, pp. 492–505, 2018.
 - [51] C. Ancuti, C. O. Ancuti, R. Timofte, and C. D. Vleeschouwer, “I-haze: a dehazing benchmark with real hazy and haze-free indoor images,” in

International Conference on Advanced Concepts for Intelligent Vision Systems. Springer, 2018, pp. 620–631.

- [52] C. O. Ancuti, C. Ancuti, R. Timofte, and C. De Vleeschouwer, “O-haze: a dehazing benchmark with real hazy and haze-free outdoor images,” in *Proceedings of the IEEE conference on computer vision and pattern recognition workshops*, 2018, pp. 754–762.
- [53] C. Ancuti, C. O. Ancuti, and C. De Vleeschouwer, “D-hazy: A dataset to evaluate quantitatively dehazing algorithms,” in *2016 IEEE international conference on image processing (ICIP)*. IEEE, 2016, pp. 2226–2230.
- [54] C. Sakaridis, D. Dai, and L. Van Gool, “Semantic foggy scene understanding with synthetic data,” *International Journal of Computer Vision*, vol. 126, no. 9, pp. 973–992, 2018.
- [55] M. Cordts, M. Omran, S. Ramos, T. Rehfeld, M. Enzweiler, R. Benenson, U. Franke, S. Roth, and B. Schiele, “The cityscapes dataset for semantic urban scene understanding,” in *Proceedings of the IEEE conference on computer vision and pattern recognition*, 2016, pp. 3213–3223.
- [56] T. Pang, M. Lin, X. Yang, J. Zhu, and S. Yan, “Robustness and accuracy could be reconcilable by (Proper) definition,” in *Proceedings of the 39th International Conference on Machine Learning*, vol. 162, 17–23 Jul 2022, pp. 17 258–17 277.
- [57] A. Mittal, A. K. Moorthy, and A. C. Bovik, “No-reference image quality assessment in the spatial domain,” *IEEE Transactions on image processing*, vol. 21, no. 12, pp. 4695–4708, 2012.

TABLE I

QUANTITATIVE ATTACK RESULTS OBTAINED BY VARIOUS ATTACK FUNCTIONS ON TEST DATASETS. THE “METHOD- ϵ ” DENOTES $\epsilon = i, i \in \{2, 4, 6, 8\}$. P, N, M, G, I AND S REPRESENT THE L_P^{MSE} , A_N , L_M^{MSE} , L_G^{MSE} , L_I^{MSE} AND L_P^{SSIM} , RESPECTIVELY. PLEASE ZOOM IN TO SEE THE NUMBERS. THE BEST RESULT IN EACH METHOD IS IN BOLD.

Methods	ITS		OTS		4K		Foggy-City		I-HAZE		O-HAZE		D-Hazy	
	PSNR↑	SSIM↑	PSNR↑	SSIM↑	PSNR↑	SSIM↑	PSNR↑	SSIM↑	PSNR↑	SSIM↑	PSNR↑	SSIM↑	PSNR↑	SSIM↑
4KDehazing	26.780	0.927	28.724	0.956	21.634	0.891	31.461	0.974	16.826	0.684	20.916	0.769	23.304	0.875
4KDehazing-P2	14.700	0.724	16.815	0.798	13.153	0.700	15.626	0.817	16.686	0.614	20.129	0.736	10.302	0.558
4KDehazing-P4	12.465	0.645	14.385	0.709	8.985	0.508	13.538	0.739	16.244	0.541	18.818	0.660	9.000	0.504
4KDehazing-P6	11.291	0.586	13.709	0.655	7.332	0.384	12.768	0.683	15.737	0.477	17.707	0.590	8.475	0.448
4KDehazing-P8	10.545	0.533	13.181	0.605	6.617	0.315	12.355	0.634	15.235	0.426	16.744	0.533	8.061	0.426
4KDehazing-N8	23.407	0.776	26.251	0.772	20.378	0.754	21.061	0.768	16.737	0.582	20.736	0.729	19.327	0.695
4KDehazing-M8	12.213	0.631	15.697	0.745	9.177	0.586	13.845	0.780	15.811	0.512	17.427	0.600	9.597	0.582
4KDehazing-G8	10.131	0.505	11.845	0.532	7.031	0.359	12.250	0.625	13.335	0.394	14.950	0.537	6.713	0.278
4KDehazing-I8	12.725	0.648	16.470	0.761	12.001	0.645	14.900	0.709	15.834	0.587	17.274	0.695	9.985	0.568
4KDehazing-S8	12.381	0.357	13.436	0.424	10.547	0.193	13.273	0.433	15.589	0.254	17.733	0.259	9.135	0.101
AODNet	19.361	0.828	23.226	0.914	14.492	0.754	20.474	0.875	15.401	0.656	18.219	0.724	16.015	0.729
AODNet-P2	19.294	0.787	23.098	0.868	13.572	0.659	18.300	0.777	15.387	0.625	18.184	0.698	15.112	0.595
AODNet-P4	19.099	0.701	22.747	0.765	11.726	0.553	15.188	0.603	15.343	0.555	18.079	0.639	13.685	0.475
AODNet-P6	18.800	0.613	22.237	0.660	10.399	0.460	13.091	0.411	15.258	0.480	17.914	0.571	12.520	0.384
AODNet-P8	18.422	0.538	21.628	0.569	9.622	0.398	11.875	0.288	15.146	0.416	17.688	0.506	11.640	0.308
AODNet-N8	19.026	0.674	22.610	0.733	13.600	0.528	18.820	0.663	15.320	0.535	18.033	0.618	14.900	0.416
AODNet-M8	18.642	0.622	22.109	0.721	10.379	0.480	14.886	0.670	15.163	0.436	17.734	0.528	12.562	0.439
AODNet-G8	16.532	0.628	19.215	0.741	8.345	0.412	10.611	0.297	13.820	0.473	16.397	0.476	8.982	0.328
AODNet-I8	18.087	0.798	22.545	0.890	13.672	0.667	16.620	0.801	15.204	0.643	18.956	0.735	13.074	0.595
AODNet-S8	18.481	0.512	21.628	0.555	12.646	0.317	15.191	0.288	15.113	0.380	17.627	0.457	13.892	0.188
DM2FNet	29.922	0.954	29.323	0.957	26.651	0.943	32.582	0.971	17.368	0.711	23.519	0.754	28.252	0.937
DM2FNet-P2	13.782	0.681	17.343	0.802	11.769	0.687	15.978	0.821	15.372	0.661	16.059	0.604	8.385	0.404
DM2FNet-P4	11.912	0.610	15.160	0.709	9.288	0.564	14.694	0.762	13.999	0.595	12.435	0.508	7.100	0.296
DM2FNet-P6	11.423	0.593	14.596	0.657	8.856	0.511	14.275	0.708	13.916	0.561	11.454	0.475	6.823	0.274
DM2FNet-P8	11.214	0.570	14.464	0.617	8.624	0.476	14.010	0.650	13.265	0.495	10.899	0.454	6.813	0.268
DM2FNet-N8	24.479	0.785	27.437	0.783	22.250	0.720	25.088	0.766	16.921	0.625	23.200	0.685	18.877	0.594
DM2FNet-M8	11.983	0.652	15.766	0.736	10.397	0.644	14.874	0.792	14.338	0.608	12.485	0.539	8.746	0.540
DM2FNet-G8	11.073	0.556	10.479	0.371	7.933	0.427	13.763	0.642	11.893	0.442	10.785	0.421	6.537	0.235
DM2FNet-I8	12.207	0.644	16.285	0.748	12.367	0.634	14.852	0.754	14.681	0.558	15.541	0.640	9.729	0.582
DM2FNet-S8	11.411	0.397	12.691	0.409	9.542	0.328	14.699	0.433	15.561	0.388	14.851	0.509	8.142	0.081
FFANet	29.414	0.962	29.839	0.959	24.641	0.936	35.053	0.981	16.507	0.749	22.587	0.853	27.441	0.919
FFANet-P2	14.450	0.682	18.130	0.822	13.027	0.678	14.805	0.784	16.432	0.680	21.548	0.816	8.959	0.461
FFANet-P4	11.498	0.523	15.911	0.735	10.473	0.558	13.312	0.654	16.250	0.567	19.989	0.737	7.347	0.312
FFANet-P6	10.528	0.474	14.657	0.663	9.199	0.477	11.752	0.486	15.990	0.472	18.498	0.655	6.885	0.255
FFANet-P8	10.091	0.448	13.978	0.611	8.742	0.441	9.728	0.326	15.664	0.400	17.487	0.579	6.556	0.223
FFANet-N8	23.930	0.754	26.790	0.805	19.497	0.712	16.832	0.699	16.398	0.633	22.085	0.767	16.028	0.544
FFANet-M8	11.553	0.586	15.514	0.735	11.766	0.646	12.403	0.597	15.968	0.536	19.053	0.648	8.841	0.457
FFANet-G8	10.063	0.437	12.279	0.537	8.726	0.448	9.760	0.326	14.010	0.499	15.938	0.601	6.552	0.227
FFANet-I8	12.386	0.653	16.608	0.771	12.805	0.613	14.899	0.718	15.690	0.688	19.412	0.717	10.338	0.528
FFANet-S8	11.072	0.245	14.456	0.438	11.359	0.273	8.702	0.187	15.554	0.283	19.492	0.343	9.615	0.022
GCANet	25.880	0.895	27.808	0.943	23.266	0.880	31.541	0.968	16.535	0.669	20.599	0.717	24.209	0.881
GCANet-P2	11.879	0.537	14.744	0.719	13.274	0.682	14.901	0.787	16.565	0.632	18.211	0.680	9.665	0.557
GCANet-P4	8.981	0.359	10.760	0.527	9.798	0.537	12.006	0.652	14.571	0.547	16.686	0.609	8.203	0.458
GCANet-P6	7.925	0.301	9.336	0.448	8.574	0.459	10.931	0.568	14.106	0.484	14.967	0.512	7.395	0.392
GCANet-P8	7.530	0.283	8.733	0.407	7.990	0.409	10.433	0.516	13.353	0.424	14.200	0.455	6.932	0.354
GCANet-N8	25.166	0.833	26.275	0.837	22.037	0.778	25.270	0.855	16.441	0.644	20.222	0.694	17.706	0.717
GCANet-M8	9.485	0.453	10.803	0.598	10.050	0.554	12.971	0.742	14.409	0.540	15.389	0.519	8.410	0.502
GCANet-G8	7.111	0.299	7.557	0.272	7.789	0.421	10.538	0.522	11.907	0.422	13.990	0.465	6.822	0.346
GCANet-I8	13.433	0.645	17.739	0.755	12.010	0.599	15.656	0.726	15.843	0.585	17.659	0.600	10.492	0.563
GCANet-S8	7.904	0.198	10.084	0.334	10.742	0.153	12.866	0.342	14.834	0.219	16.660	0.208	8.989	0.185
GridDehazeNet	23.243	0.934	27.806	0.961	22.614	0.935	30.508	0.961	15.872	0.676	19.543	0.798	24.649	0.892
GridDehazeNet-P2	16.826	0.763	18.854	0.842	15.632	0.784	15.279	0.787	15.828	0.613	19.264	0.695	9.332	0.585
GridDehazeNet-P4	13.636	0.634	16.447	0.756	12.155	0.660	14.300	0.718	15.713	0.505	18.597	0.565	8.067	0.459
GridDehazeNet-P6	12.342	0.561	15.269	0.688	10.504	0.575	13.521	0.654	15.536	0.414	17.714	0.459	7.268	0.389
GridDehazeNet-P8	11.718	0.512	14.420	0.628	9.694	0.517	12.932	0.597	15.319	0.348	16.838	0.380	6.753	0.356
GridDehazeNet-N8	22.304	0.792	25.974	0.802	20.384	0.754	17.223	0.735	15.832	0.622	19.350	0.722	10.531	0.583
GridDehazeNet-M8	13.064	0.635	16.758	0.766	12.348	0.700	14.150	0.774	15.521	0.465	17.771	0.478	7.698	0.509
GridDehazeNet-G8	11.956	0.581	12.156	0.547	9.416	0.491	12.700	0.586	14.011	0.434	14.950	0.429	6.714	0.354
GridDehazeNet-I8	12.831	0.656	16.928	0.778	12.280	0.658	14.906	0.730	15.933	0.676	19.800	0.711	10.083	0.540
GridDehazeNet-S8	13.083	0.395	13.476	0.435	13.179	0.341	14.618	0.420	15.189	0.264	17.243	0.173	9.337	0.158
MSBDN	24.229	0.903	24.229	0.903	23.785	0.904	30.382	0.969	17.074	0.505	20.450	0.579	23.093	0.884
MSBDN-P2	</													

TABLE II

QUANTITATIVE DEFENSE RESULTS OBTAINED BY L_{def}^P AND L_{def}^G ON TEST DATASETS. P AND G REPRESENT ATTACK LOSS L_P AND L_G , RESPECTIVELY. THE “METHOD-P ϵ ” AND “METHOD-G ϵ ” DENOTE THE ATTACK RESULTS WHEN $\epsilon = i, i \in \{2, 4, 6, 8\}$. TP DENOTES TRAINED BY L_{def}^P , AND TG MEANS TRAINED BY L_{def}^G . “METHOD: TP” AND “METHOD: TG” STAND FOR THE DEHAZING RESULTS WITH NO ATTACK ($\epsilon = 0$). PSNR AND SSIM ARE DISPLAYED IN THE FORM OF A/B, WHERE A IS THE RESULT AFTER DEFENSE TRAINING AND B IS THE RESULT BEFORE DEFENSE TRAINING. THE BOLD VALUE IN A/B (WHEN $\epsilon > 0$) REPRESENTS A BETTER DEHAZING RESULT (WORSE ATTACK RESULT).

Methods	D-Hazy		Foggy-City	
	PSNR \uparrow	SSIM \uparrow	PSNR \uparrow	SSIM \uparrow
4KDehazing: TP	15.250/ 23.304	0.745/ 0.875	24.533/ 31.461	0.912/ 0.974
4KDehazing-P2	15.313 /10.302	0.739 /0.558	24.413 /15.626	0.906 /0.817
4KDehazing-P4	15.317 /9.000	0.705 /0.504	23.918 /13.538	0.884 /0.739
4KDehazing-P6	15.248 /8.475	0.648 /0.448	23.193 /12.768	0.850 /0.683
4KDehazing-P8	15.115 /8.061	0.576 /0.426	22.501 /12.355	0.803 /0.634
4KDehazing: TG	15.532/ 23.304	0.753/ 0.875	24.458/ 31.461	0.909/ 0.974
4KDehazing-G2	15.142 /9.363	0.732 /0.437	23.390 /15.273	0.893 /0.792
4KDehazing-G4	14.753 /7.574	0.704 /0.324	22.227 /13.142	0.868 /0.711
4KDehazing-G6	14.374 /6.983	0.672 /0.293	21.168 /12.567	0.837 /0.667
4KDehazing-G8	14.005 /6.713	0.636 /0.278	20.256 /12.250	0.800 /0.625
AODNet: TP	15.545/ 16.015	0.746 /0.729	19.737/ 20.474	0.863/ 0.875
AODNet-P2	15.318 /15.112	0.601 /0.595	19.674 /18.300	0.816 /0.777
AODNet-P4	14.862 /13.685	0.467/ 0.475	19.462 /15.188	0.724 /0.603
AODNet-P6	14.308 /12.520	0.374/ 0.384	19.127 /13.091	0.625 /0.411
AODNet-P8	13.691 /11.640	0.309 /0.308	18.707 /11.875	0.538 /0.288
AODNet: TG	15.203/ 16.015	0.736 /0.729	19.615/ 20.474	0.860/ 0.875
AODNet-G2	14.425 /13.341	0.655 /0.606	19.069 /16.439	0.827 /0.761
AODNet-G4	13.667 /11.367	0.547 /0.495	18.518 /13.454	0.767 /0.596
AODNet-G6	12.967 /9.959	0.453 /0.408	17.978 /11.608	0.684 /0.412
AODNet-G8	12.336 /8.982	0.376 /0.328	17.464 /10.611	0.589 /0.297
GCANet: TP	22.974/ 24.209	0.843/ 0.881	30.063/ 31.541	0.957/ 0.968
GCANet-P2	15.463 /9.665	0.736 /0.557	23.486 /14.901	0.895 /0.787
GCANet-P4	15.074 /8.20	0.712 /0.458	22.581 /12.006	0.872 /0.652
GCANet-P6	14.645 /7.395	0.683 /0.392	21.701 /10.931	0.842 /0.568
GCANet-P8	14.253 /6.932	0.650 /0.354	20.879 /10.433	0.805 /0.516
GCANet: TG	22.655/ 24.209	0.836/ 0.881	30.335/ 31.541	0.958/ 0.968
GCANet-G2	15.358 /9.505	0.727 /0.545	23.461 /14.921	0.894 /0.785
GCANet-G4	14.922 /8.052	0.701 /0.443	22.480 /12.107	0.871 /0.653
GCANet-G6	14.475 /7.283	0.671 /0.381	21.562 /11.050	0.841 /0.573
GCANet-G8	14.070 /6.822	0.639 /0.346	20.722 /10.538	0.806 /0.522
GridDehazeNet: TP	24.261/ 24.649	0.869/ 0.892	29.970/ 30.508	0.957/ 0.961
GridDehazeNet-P2	14.795 /9.332	0.722 /0.585	21.059 /15.279	0.850 /0.787
GridDehazeNet-P4	14.705 /8.067	0.708 /0.459	20.406 /14.300	0.819 /0.718
GridDehazeNet-P6	15.085 /7.268	0.690 /0.389	19.825 /13.521	0.782 /0.654
GridDehazeNet-P8	14.824 /6.753	0.656 /0.356	19.207 /12.932	0.740 /0.597
GridDehazeNet: TG	24.834 /24.649	0.885/ 0.892	29.753/ 30.508	0.956/ 0.961
GridDehazeNet-G2	15.626 /9.316	0.732 /0.585	20.773 /15.082	0.855 /0.781
GridDehazeNet-G4	15.402 /8.028	0.713 /0.457	20.144 /13.924	0.829 /0.704
GridDehazeNet-G6	15.114 /7.226	0.687 /0.388	19.579 /13.220	0.795 /0.641
GridDehazeNet-G8	14.690 /6.714	0.653 /0.354	19.011 /12.700	0.753 /0.586
MSBDN: TP	22.771/ 23.093	0.865/ 0.884	29.370/ 30.382	0.964/ 0.969
MSBDN-P2	16.068 /9.510	0.746 /0.561	23.380 /15.824	0.887 /0.788
MSBDN-P4	15.428 /7.422	0.715 /0.401	22.211 /12.874	0.865 /0.643
MSBDN-P6	14.836 /6.594	0.676 /0.333	21.218 /11.814	0.839 /0.555
MSBDN-P8	14.311 /6.215	0.634 /0.296	20.427 /11.148	0.811 /0.491
MSBDN: TG	22.399/ 23.093	0.864/ 0.884	29.671/ 30.382	0.964/ 0.969
MSBDN-G2	15.723 /8.827	0.739 /0.485	23.421 /15.411	0.888 /0.770
MSBDN-G4	15.063 /6.858	0.704 /0.330	22.139 /12.277	0.866 /0.586
MSBDN-G6	14.469 /6.156	0.665 /0.261	21.101 /11.216	0.839 /0.492
MSBDN-G8	13.950 /5.738	0.624 /0.226	20.269 /10.713	0.812 /0.442

TABLE III

QUANTITATIVE ATTACK RESULTS OBTAINED BY L_P^{MSE} ON D-HAZY. THE “METHOD-AI*k*” DENOTES THE ATTACK RESULTS WHEN ATTACK ITERATIONS (AI) ARE $k = i, i \in \{1, 2, 3, 5, 10, 15, 20, 25, 30\}$. “METHOD” MEANS THE DEHAZING RESULTS WITHOUT ATTACK. ϵ IS 4. THE BOLD VALUE REPRESENTS A BETTER ATTACK RESULT (WORSE DEHAZING RESULT).

Methods	D-Hazy	
	PSNR \uparrow	SSIM \uparrow
4KDehazing	23.304	0.875
4KDehazing-AI1	14.534	0.668
4KDehazing-AI2	11.143	0.596
4KDehazing-AI3	10.057	0.560
4KDehazing-AI5	9.536	0.534
4KDehazing-AI10	8.918	0.493
4KDehazing-AI15	8.839	0.482
4KDehazing-AI20	8.462	0.474
4KDehazing-AI25	8.464	0.460
4KDehazing-AI30	8.397	0.467
AODNet	16.015	0.729
AODNet-AI1	15.054	0.472
AODNet-AI2	14.657	0.451
AODNet-AI3	14.447	0.455
AODNet-AI5	14.073	0.463
AODNet-AI10	13.683	0.475
AODNet-AI15	13.539	0.482
AODNet-AI20	13.435	0.486
AODNet-AI25	13.375	0.488
AODNet-AI30	13.353	0.490
GCANet	24.209	0.881
GCANet-AI1	12.088	0.649
GCANet-AI2	9.996	0.547
GCANet-AI3	9.307	0.510
GCANet-AI5	8.701	0.477
GCANet-AI10	8.148	0.451
GCANet-AI15	7.988	0.442
GCANet-AI20	7.837	0.437
GCANet-AI25	7.750	0.432
GCANet-AI30	7.725	0.431
GridDehazeNet	24.649	0.892
GridDehazeNet-AI1	9.969	0.599
GridDehazeNet-AI2	9.346	0.570
GridDehazeNet-AI3	9.063	0.548
GridDehazeNet-AI5	8.647	0.514
GridDehazeNet-AI10	8.080	0.459
GridDehazeNet-AI15	7.830	0.434
GridDehazeNet-AI20	7.649	0.417
GridDehazeNet-AI25	7.538	0.407
GridDehazeNet-AI30	7.446	0.398
MSBDN	23.093	0.884
MSBDN-AI1	13.056	0.639
MSBDN-AI2	9.703	0.532
MSBDN-AI3	8.667	0.493
MSBDN-AI5	7.997	0.443
MSBDN-AI10	7.492	0.421
MSBDN-AI15	7.413	0.408
MSBDN-AI20	7.305	0.399
MSBDN-AI25	7.239	0.389
MSBDN-AI30	7.285	0.396

TABLE IV

QUANTITATIVE DEFENSE RESULTS OBTAINED BY L_{def}^P ON D-HAZY. THE ATTACK LOSS IS L_P^{MSE} . THE “METHOD-AI*k*” DENOTES THE ATTACK RESULTS WHEN ATTACK ITERATIONS (AI) ARE $k = i, i \in \{1, 2, 3, 5, 10, 15, 20, 25, 30\}$. “METHOD” MEANS THE DEHAZING RESULTS WITHOUT ATTACK. ϵ IS 4. PSNR AND SSIM ARE DISPLAYED IN THE FORM OF A/B, WHERE A IS THE RESULT AFTER DEFENSE TRAINING (THE k FOR DEFENSE TRAINING IS RANDOMLY SELECTED FROM $\{20, 25, 30\}$) AND B IS THE RESULT BEFORE DEFENSE TRAINING. THE BOLD VALUE IN A/B REPRESENTS A BETTER DEHAZING RESULT (WORSE ATTACK RESULT).

Methods	D-Hazy	
	PSNR \uparrow	SSIM \uparrow
4KDehazing	15.172/ 23.304	0.747/ 0.875
4KDehazing-AI1	15.142 /14.534	0.693 /0.668
4KDehazing-AI2	15.131 /11.143	0.669 /0.596
4KDehazing-AI3	15.131 /10.057	0.658 /0.560
4KDehazing-AI5	15.135 /9.536	0.653 /0.534
4KDehazing-AI10	15.156 /8.918	0.658 /0.493
4KDehazing-AI15	15.164 /8.839	0.662 /0.482
4KDehazing-AI20	15.170 /8.462	0.665 /0.474
4KDehazing-AI25	15.174 /8.464	0.667 /0.460
4KDehazing-AI30	15.174 /8.397	0.668 /0.467
AODNet	15.458/ 16.015	0.739 /0.729
AODNet-AI1	15.014/ 15.054	0.475 /0.472
AODNet-AI2	14.887 /14.657	0.451 / 0.451
AODNet-AI3	14.873 /14.447	0.450/ 0.455
AODNet-AI5	14.855 /14.073	0.451/ 0.463
AODNet-AI10	14.816 /13.683	0.454/ 0.475
AODNet-AI15	14.794 /13.539	0.457/ 0.482
AODNet-AI20	14.783 /13.435	0.459/ 0.486
AODNet-AI25	14.770 /13.375	0.461/ 0.488
AODNet-AI30	14.768 /13.353	0.463/ 0.490
GCANet	22.829/ 24.209	0.838/ 0.881
GCANet-AI1	15.752 /12.088	0.733 /0.649
GCANet-AI2	15.457 /9.996	0.725 /0.547
GCANet-AI3	15.247 /9.307	0.718 /0.510
GCANet-AI5	15.057 /8.701	0.710 /0.477
GCANet-AI10	15.009 /8.148	0.708 /0.451
GCANet-AI15	15.001 /7.988	0.708 /0.442
GCANet-AI20	15.000 /7.837	0.708 /0.437
GCANet-AI25	15.003 /7.750	0.708 /0.432
GCANet-AI30	15.000 /7.725	0.708 /0.431
GridDehazeNet	24.840 /24.649	0.890/ 0.892
GridDehazeNet-AI1	15.687 /9.969	0.735 /0.599
GridDehazeNet-AI2	15.533 /9.346	0.729 /0.570
GridDehazeNet-AI3	15.453 /9.063	0.724 /0.548
GridDehazeNet-AI5	15.400 /8.647	0.721 /0.514
GridDehazeNet-AI10	15.372 /8.080	0.720 /0.459
GridDehazeNet-AI15	15.370 /7.830	0.720 /0.434
GridDehazeNet-AI20	15.365 /7.649	0.720 /0.417
GridDehazeNet-AI25	15.365 /7.538	0.720 /0.407
GridDehazeNet-AI30	15.363 /7.446	0.720 /0.398
MSBDN	17.109/ 23.093	0.779/ 0.884
MSBDN-AI1	16.921 /13.056	0.708 /0.639
MSBDN-AI2	16.749 /9.703	0.683 /0.532
MSBDN-AI3	16.702 /8.667	0.681 /0.493
MSBDN-AI5	16.535 /7.997	0.693 /0.443
MSBDN-AI10	16.289 /7.492	0.714 /0.421
MSBDN-AI15	16.371 /7.413	0.719 /0.408
MSBDN-AI20	16.340 /7.305	0.724 /0.399
MSBDN-AI25	16.314 /7.239	0.725 /0.389
MSBDN-AI30	16.262 /7.285	0.727 /0.396